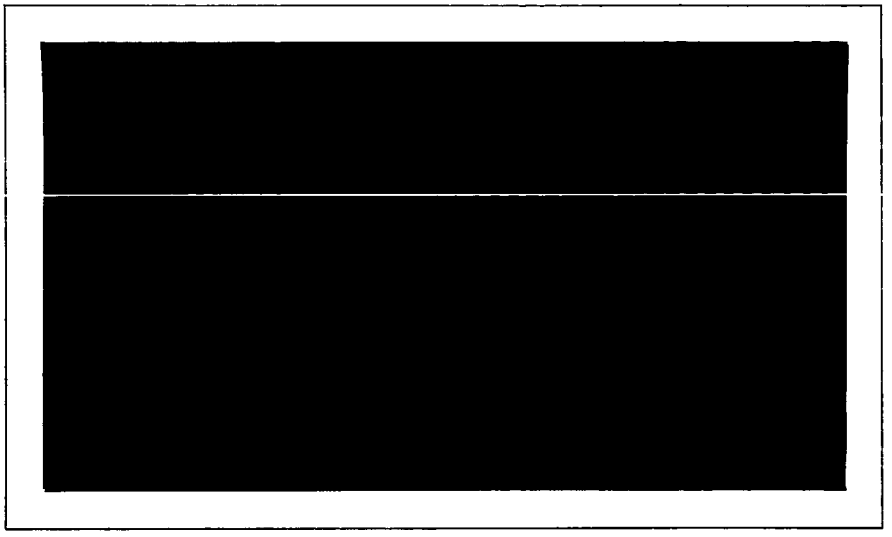

UNIVERSITY OF PENNSYLVANIA

ELECTROCHEMISTRY LABORATORY

PHILADELPHIA, PENNSYLVANIA 19104

REPORT NO. 7

QUARTERLY PROGRESS REPORT

1 OCTOBER 1965 to 31 DECEMBER 1965

STUDIES IN FUNDAMENTAL CHEMISTRY OF FUEL CELL REACTIONS

NsG-325

Submitted to:

NATIONAL AERONAUTICS AND SPACE ADMINISTRATION

Washington 25, D. C.

Submitted by:

Professor John O'M. Bockris

The Electrochemistry Laboratory
The University of Pennsylvania
Philadelphia, Pa. 19104

NOTICE

This report was prepared as an account of Government sponsored work. Neither the United States, nor the National Aeronautics and Space Administration (NASA), nor any person acting on behalf of NASA:

A.) Makes any warranty or representation, expressed or implied, with respect to the accuracy, completeness, or usefulness of the information contained in this report, or that the use of any information, apparatus, method, or process disclosed in this report may not infringe privately owned rights; or

B.) Assumes any liabilities with respect to the use of or for damages resulting from the use of any information, apparatus, method or process disclosed in this report.

As used above, "person acting on behalf of NASA" includes any employee or contractor of NASA, or employee of such contractor, to the extent that such employee or contractor of NASA, or employee of such contractor prepares, disseminates, or provides access to, any information pursuant to his employment or contract with NASA, or his employment with such contractor.

TABLE OF CONTENTS

PROJECT PERSONNEL

Section I

Mr. Boris Cahan, Pre Doctoral Research Fellow

Dr. Halina Wroblowa, Supervisor

Section II

Miss Rowshan Jahan, Pre Doctoral Research Fellow

Dr. Aleksandar Damjanovic, Supervisor

Section III

Mr. Shyam Argade, Pre Doctoral Research Fellow

Dr. Eliezer Gileadi, Supervisor

Section IV

Dr. Ljerka Duic, Post Doctoral Research Fellow

Dr. Halina Wroblowa, Supervisor

Section V

Dr. S. Srinivasan, Post Doctoral Research Fellow

Dr. John O'M. Bockris, Supervisor

ABSTRACTS

SECTION I. THE MECHANISM OF VARIOUS TYPES OF HIGH RATE ELECTRODES

The shape of the meniscus in the model porous electrode and the contact angle have been determined by two methods: interferometry and reflection technique. Numerical solutions of equations set up for a finite contact angle model, taking into account resistance, diffusion and activation control have been obtained. The calculated current-potential relations were in extremely good agreement with experimental results obtained for H_2 ionization and O_2 reduction reactions.

The electrochemical behavior in the model pore is extremely sensitive to the contact angle. Very high local current density over small parts of the meniscus indicates the possibility of utilizing extremely small amounts of catalyst to obtain relatively high power from a porous electrode.

SECTION II. THE MECHANISM OF ELECTROCATALYSIS

The catalytic activity of simple electrode reactions (H_2/H^+; Fe^{2+}/Fe^{3+}) is studied on a number of alloys. Data are given for hydrogen evolution reaction on a series of Pt-Ni, and for Fe^{3+}/Fe^{2+} on Au-Pd alloys. In the latter, exchange current density first increases and then decreases with increasing at % of Au in alloys. Maximum appears to occur at the point where d-band is expected to be filled.

III. THE ELECTRICAL DOUBLE LAYER AT THE SOLID-SOLUTION INTERFACE

Capacitance behavior of gold electrodes in dilute solutions was studied under high purity conditions. The minimum in the capacity-potential curve in a 10^{-3} N $HClO_4$ solution was found to be at + 170 mv (N.H.E.). It was observed that the potential of zero charge did not vary with pH in acidic solutions. At pH 9 the potential of zero charge was found to be + 10 mv (N.H.E.). Although a slight variation in capacitance with frequency was found, the position of potential of zero charge was independent of frequency.

SECTION IV. ADSORPTION IN THE DOUBLE LAYER WITH SPECIAL REFERENCE TO THERMAL EFFECTS

Potential sweep method of measuring adsorption was utilized to obtain data on adsorption of ethylene and benzene as a function of potential. Results have been compared with those obtained by radio-tracer method. Analysis of the agreements and discrepancies observed is under way.

Section V. Electrode Kinetic Aspects of Electrochemical Energy Conversion

Expressions for the current distribution and overpotential as a function of current density are derived for the simple pore model of the porous electrode assuming all forms of polarization and for the cases of activation-concentration and of activation-ohmic polarization. It is shown that the one dimensional treatment is applicable up to one-tenth of the limiting current for the case of activation-concentration polarization. By using the numerical values of the variousparameter (e.g., diffusion coefficient solubility of reactant gas in electrolyte, exchange current density, specific conductance of electrolyte) it is shown that the case of all forms of polarization reduces to that of activation-concentration polarization. The case of activation-ohmic polarization shows the interesting result that current densities can be increased by a factor of 10^3 times if concentration polarization is eliminated, for example, by using very soluble fuels or by circulating the electrolyte saturated with the reactant through the porous electrode.

SECTION I: THE MECHANISM OF VARIOUS TYPES OF HIGH RATE ELECTRODES

The object of the investigation of the model porous electrode during the report period was twofold:

1. Obtain current-potential characteristics for a reaction with exchange current much lower than that of H_2.

2. Mapping of the interface by means of optical methods.

These objectives were investigated as follows:

1. Oxygen reduction was studied under purified conditions. Although the exchange current is some 10^7 times less than that of H_2, the general characteristic, namely the linearity of current-potential relations is the same (see Figs. 1 and 1a, full lines). The slope dV/dI depends on the height of the meniscus in the slot, increasing with increase of path length.

2. The optical methods were used: (a) reflection study; (b) interferometry.

The interferometric technique

The optically flat surface of the electrode provides one plane for interference (this corresponds to the reference plane in the interferometer). The liquid-gas interfaee is the other plane. Directing NaD light at this interface, an interference pattern is set up, with dark fringes at positions where $2\,nd = m\lambda$, (d = thickness of meniscus, λ = wave-length; m = 0, 1, 2, 3.....; n = refractive index $\approx$ 1.31).

The interference patterns at the meniscus were photographed

with 50 X magnification.

The reflection technique

This is illustrated in Figure 2. The light from a point source is directed at the interface and reflected into the microscope directed at 90° to the Pt surface. Thus, beams reflected from points above the curvature of meniscus can be seen only if the angle of incidence $\theta = 0^{\circ}$; at larger angles (position 1, Fig. 2) no reflection is seen in the microscope. Raising the light source a point is reached, where the reflected beam first appears in the microscope, indicating the beginning of the detectable curvature of the meniscus. Measuring the angle 2θ by reflection of the beam from several points on the meniscus curvature, its shape was determined over 125μ of the meniscus height.

Accuracy of the determination of θ

The microscope is placed on the cathetometer stand at the distance of 10 cm from the Pt surface. The angle θ is given by $\tan 2\theta = h/10$. The height, h, can be measured with an accuracy of $\pm 10^{-2}$ cm. Another source of error is the angle of the acceptance of the microscope, which is 0.035°.

Thus the accuracy of the measurement is

$$\Delta \tan 2\theta = \pm (10^{-3} + \tan 0.025) = \pm 0.0014$$

which corresponds to $\Delta\theta = \pm 0.04^{\circ}$.

Results and Discussion

1. The contact angle

Approaching the meniscus from above, the angle θ is continuously 0, until abruptly its value jumps to $\sim 1.5^{\circ}$, and then continuously increases. In view of the above accuracy of θ measurement - 0.04%, this indicates that there is a discontinuity at the interface, and that the meniscus ends with a finite contact angle.

The value of this angle depends on polarization.

This discontinuity reveals itself also in interferometric measurements by the abrupt black edge of the meniscus contrasting with the bright reflection from the surface above (see Fig. 3). The above picture corresponds to a wedge type film with the dark fringes at the apex ($m = 0$) and at thickness $d = m\lambda/2n$.

Meniscus shape

This was mapped on the basis of the values of θ found by reflection technique, and independently, on the basis of the thickness of the meniscus edge obtained by interferometric technique. Both data agree remarkably well (see Fig. 4), as may be seen by comparison of position of fringes observed and calculated from results obtained by reflection.

The mapped curvature fits to a cubic equation with a very small coefficient at x^3 (x - distance from top of meniscus).

Current-potential relation

A program has been set up for use with "QUIKTRAN" and/or "FORTRAN", for the solution of the differential equations for the "finite angle" meniscus. Provision has been made for studying the effects of all parameters including the shape of the meniscus, and the combination of resistance, activation and diffusional control. A quadratic equation was used to describe the shape of meniscus. The fit was good, as might be expected by the small coefficient at x^3.

The numerical solution obtained is in reasonably good agreement with experimental results (see Figs. 1, 1a) not only in that the current-potential relation is linear, but in the absolute values of currents calculated and observed.

Conclusions

1. The theoretical treatment of the finite angle meniscus model assumed on the basis of optical experiments yields current-potential relationship, as well as the absolute values of current in a remarkably good agreement with experiment.

2. Local current densities obtainable in cells corresponding to this model may be extremely high (exceeding 100 A cm^{-2}).

3. The extremely high local power densities explain completely the observed meniscus heating effect.

4. A multiporous cell satisfying the conditions of the finite angle meniscus could yield high power with extremely small amounts of catalyst.

Future Work

Further analysis of numerical results obtained from the computer will be made and dependence of current on i_o, θ and potential will be established.

An attempt will be made to construct a multiporous electrode corresponding to the investigated model.

Captions to Figures

Figure 1. Current vs voltage plot for H_2.

Figure 1a. Current vs voltage plot for O_2.

Figure 2. Geometry of the reflection technique.

Figure 3. Schematic representation of interferometric results.

Figure 4. Comparison of results obtained by reflection and interferometry.

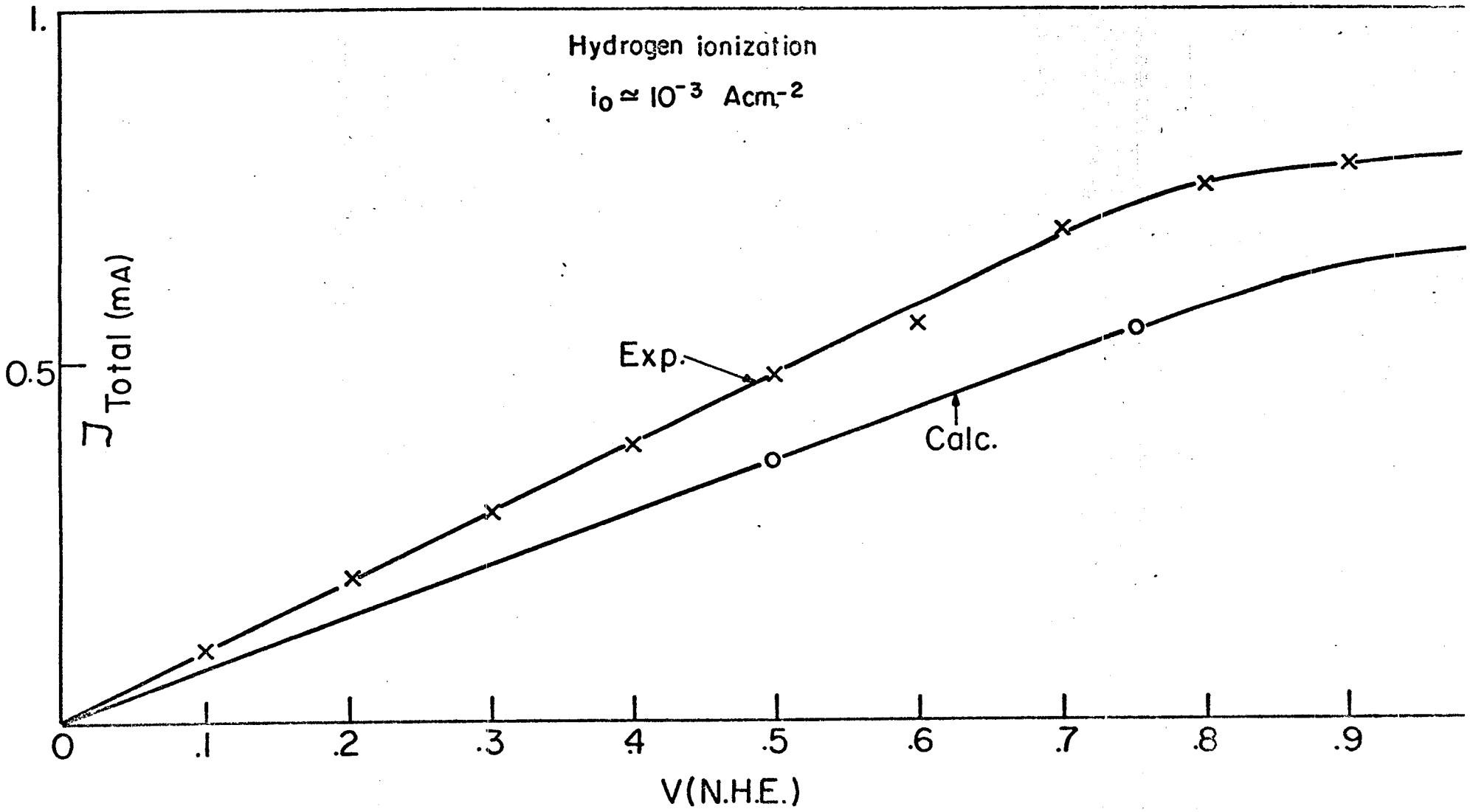

FIG. 1 Current vs. voltage plot for H_2

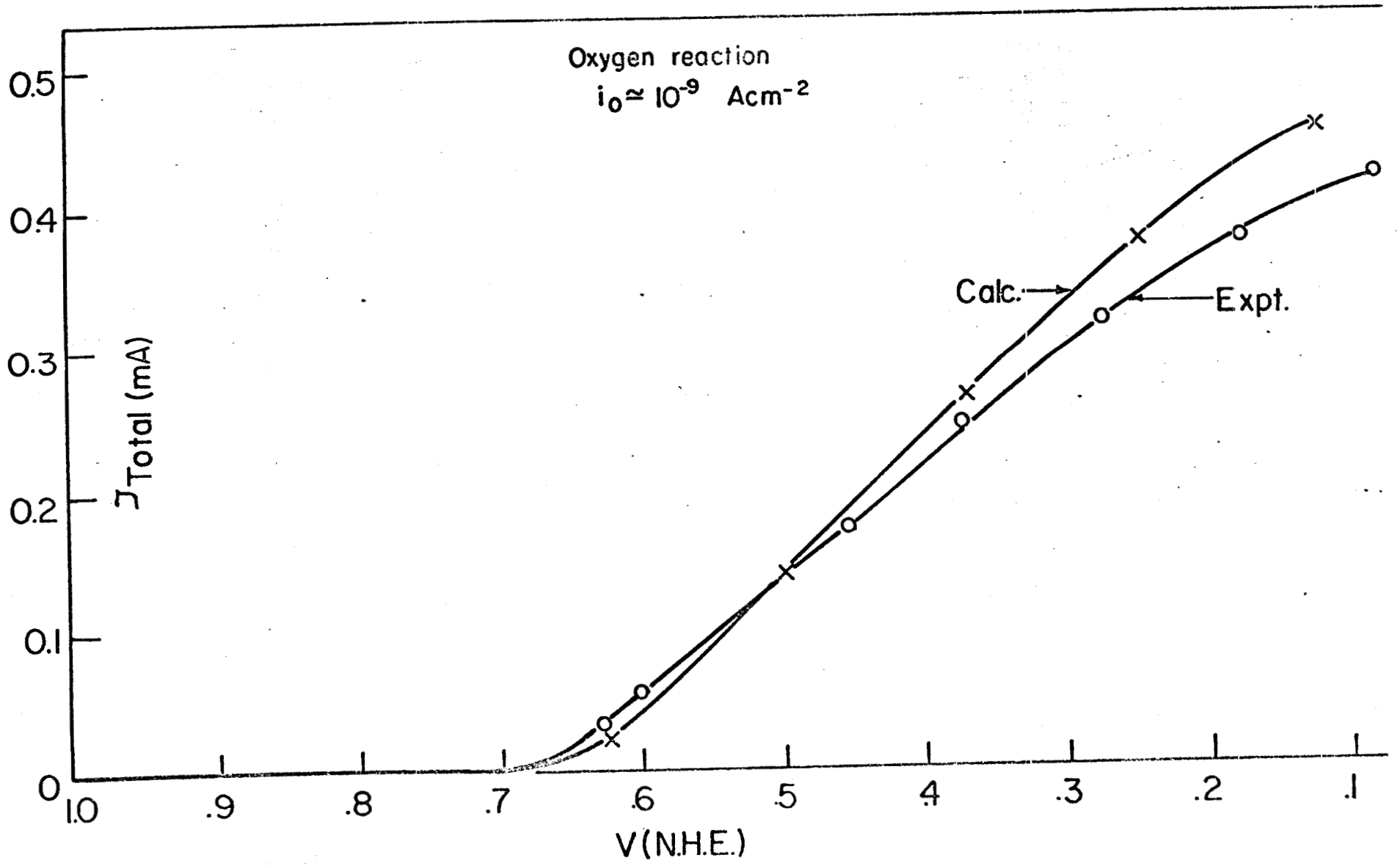

FIG. 1a Current vs. voltage plot for O_2.

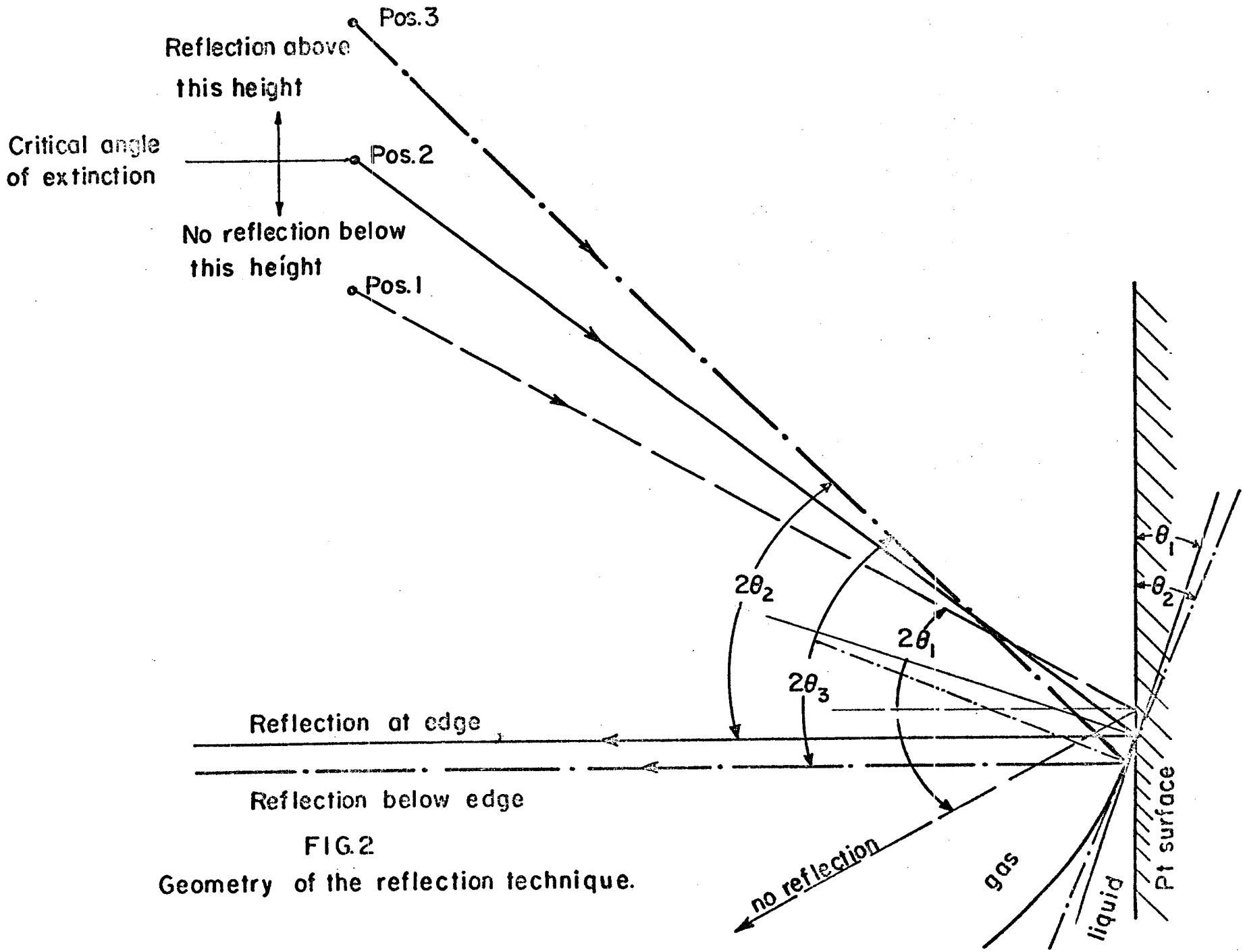

FIG.2
Geometry of the reflection technique.

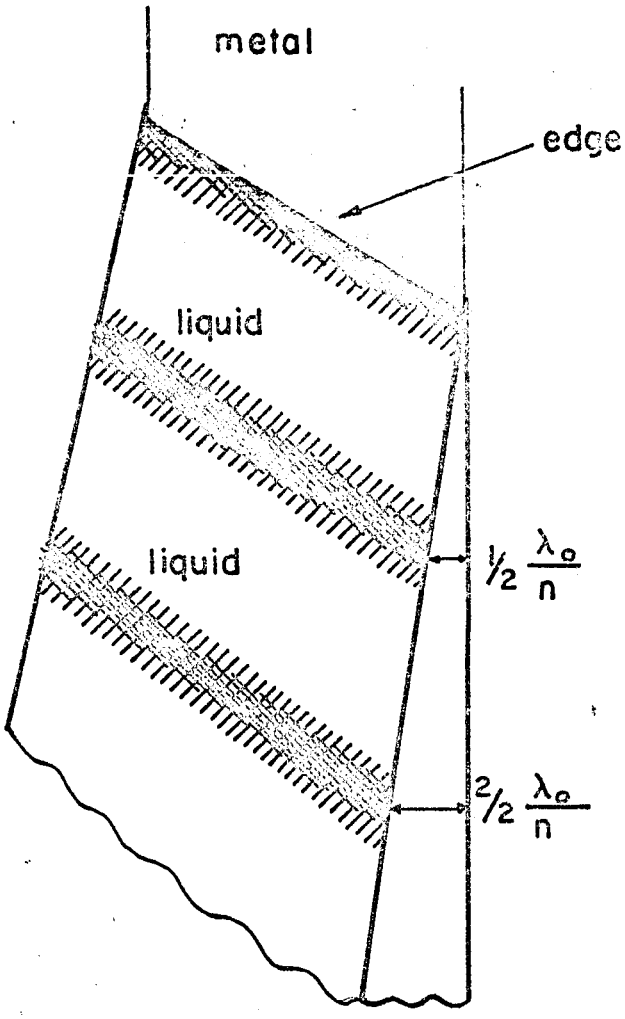

FIG. 3

Schematic representation of interferometric results.

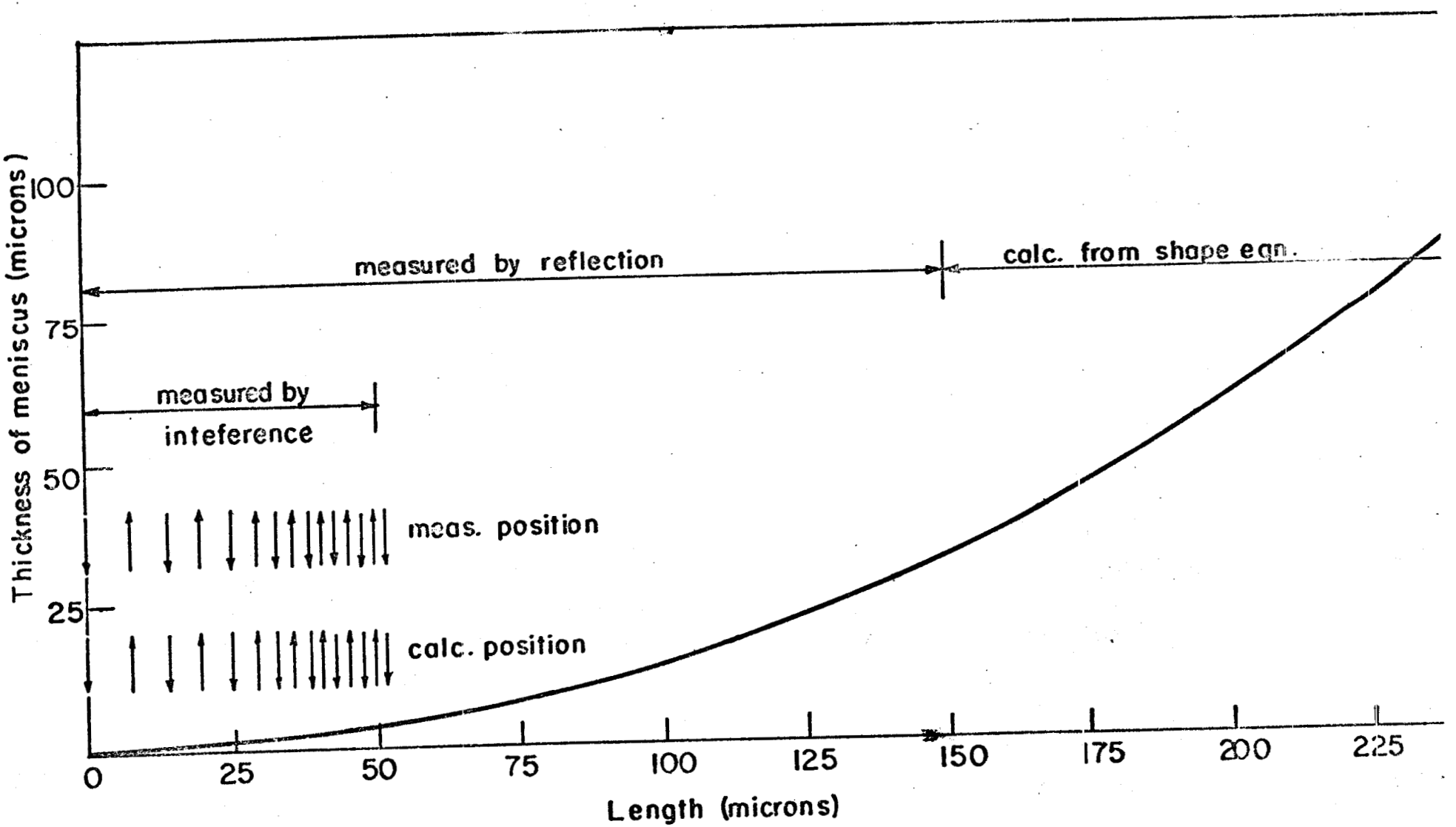

FIG. 4 Compariso of results obtained by reflection and interferometry.

II. THE MECHANISM OF ELECTROCATALYSIS

1. Introduction

Electrocatalysis of H_2/H^+ and Fe^{2+}/Fe^{3+} reactions.

Catalytic activity of simple electrode reactions, that of H_2/H^+ and Fe^{2+}/Fe^{3+}, has been studied on different electrode materials. In here, data are reported on the H_2/H^+ reaction on Pt-Ni alloy series, and of Fe^{2+}/Fe^{3+} on Au-Pd alloys.

2. Experimental and Results

A series of Pt-Ni alloys were prepared by induction heating and then by prolonged (7 days) annealing at high ($\sim 1100^{o}C$) temperature. With this annealing a complete homogenization of alloys should be achieved. Each alloy in the form of a bead was placed into Teflon holder as described in the previous report. Further treatment of the electrode, and the preparation of the solution has also been described in the previous report.[1] Special care was taken to insure that the electrode treatment does not result in separation of alloy components at the electrode surface.

In Fig. 1, the exchange current densities for H_2/H^+ are plotted versus atomic % of Ni in Pt-Ni alloys. Data are for acid solution (1 N H_2SO_4). Activity changes with atomic composition of alloys, but there is a distinct discontinuity at about 50 at %. It should be noted that the mechanism of the reaction on Ni ($b = 2RT/F$) differs from that on Pt ($RT/2F$). As would be expected, Ni-rich alloys have the same Tafel slope (and presumably the mechanism) as Ni, and Pt-rich alloys as Pt.

In Fig. 2, data on the redox Fe^{2+}/Fe^{3+} reaction are given. Exchange current densities on Au-Pd alloys (and Pt) are plotted versus lattice parameters of alloys. A line through experimental points is tentatively drawn. Were the data plotted vs. at % of the alloys, similar trend would be noticed. A characteristic of the plot is that the activity does change from one metal to another and also by alloying. Further, there appears to be a maximum in activity. It is interesting that the position of the maximum occurs at about 50 at % alloy, where it would be expected that the electronic structure of alloys changes (and the d-band of Pd becomes filled). That exchange current density does appear on electrode material is further shown in Table I in which data for B_4C, TiC and TaC are given. For Table I please see page 7a.

3. Discussion

Results on Pt-Ni are in fact similar to those on Pd-Ni alloys.[2] Thus, in the latter case (Fig. 3), linearity exists over the whole range of lattice parameters (nearly the same scale as at % of alloy, and in the former case over the end member only. The abrupt change in slope occurs at about 50 at %. This change must be due to the change in mechanism of the reaction at this alloy composition.

The question may be asked what structural or electronic properties of alloy is this linearity due to? First of all, alloying must affect exponential term in the overall rate equation. At this stage of the analysis it appears that the observed change is due to the change in the heat of H-adsorption. This would be possible if the bond strength

TABLE I

EXCHANGE CURRENT DENSITIES FOR Fe^{3+}/Fe^{2+} REACTION ON SOME CARBIDE ELECTRODES

Electrodes	io (amp/cm^2)
B_4C	6 10^{-4}
TiC	2 10^{-3}
TaC	3 10^{-4}

between metal atoms in the alloy changes linearly with the alloying. In the case of two similar atoms, as Ni and Pd, this linear change may be expected. The magnitude of change (2.5 decades from Ni to Pd) can be accounted for with the difference in heats of adsorption on Ni and Pd electrodes, as experimentally observed.[3] Change in the activity of Pt-Ni alloy can similarly be accounted for.

Dependence of the activity of Fe^{2+}/Fe^{3+} on the electrode material and on alloying is not expected in simple redox reactions, unless some interaction of reacting cations and the electrode existed. It is noteworthy that the maximum in activity occurs at the point where the electronic structure of alloys is expected to change. This strongly indicates that some electronic factors are involved in the catalysis of the Fe^{2+}/Fe^{3+} reaction. Further analysis is in progress.

4. Future Work

Further work will include more with non-noble metal alloys and special compounds such as bronzes and oxide electrodes.

References:

1. Quarterly NASA Report, No. 6, 1 July 1965 to September 1965
2. Ibid.
3. Bond, Catalysis by Metal, Academic Press (1953).

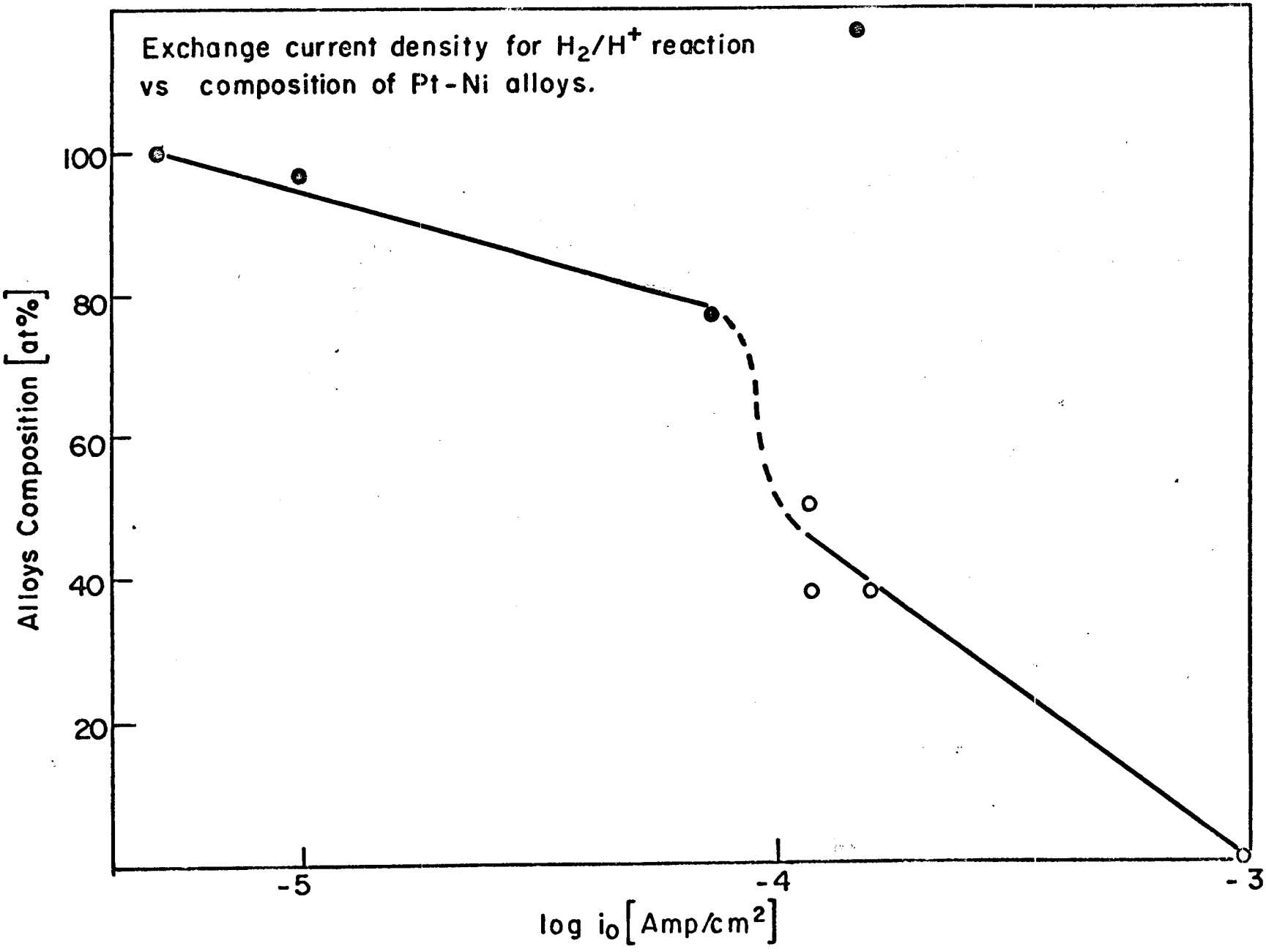
Exchange current density for H_2/H^+ reaction
vs composition of Pt-Ni alloys.
Alloys Composition [at%]
100
80
60
40
20
-5
-4
-3
log i_o [Amp/cm^2]

FIG.1

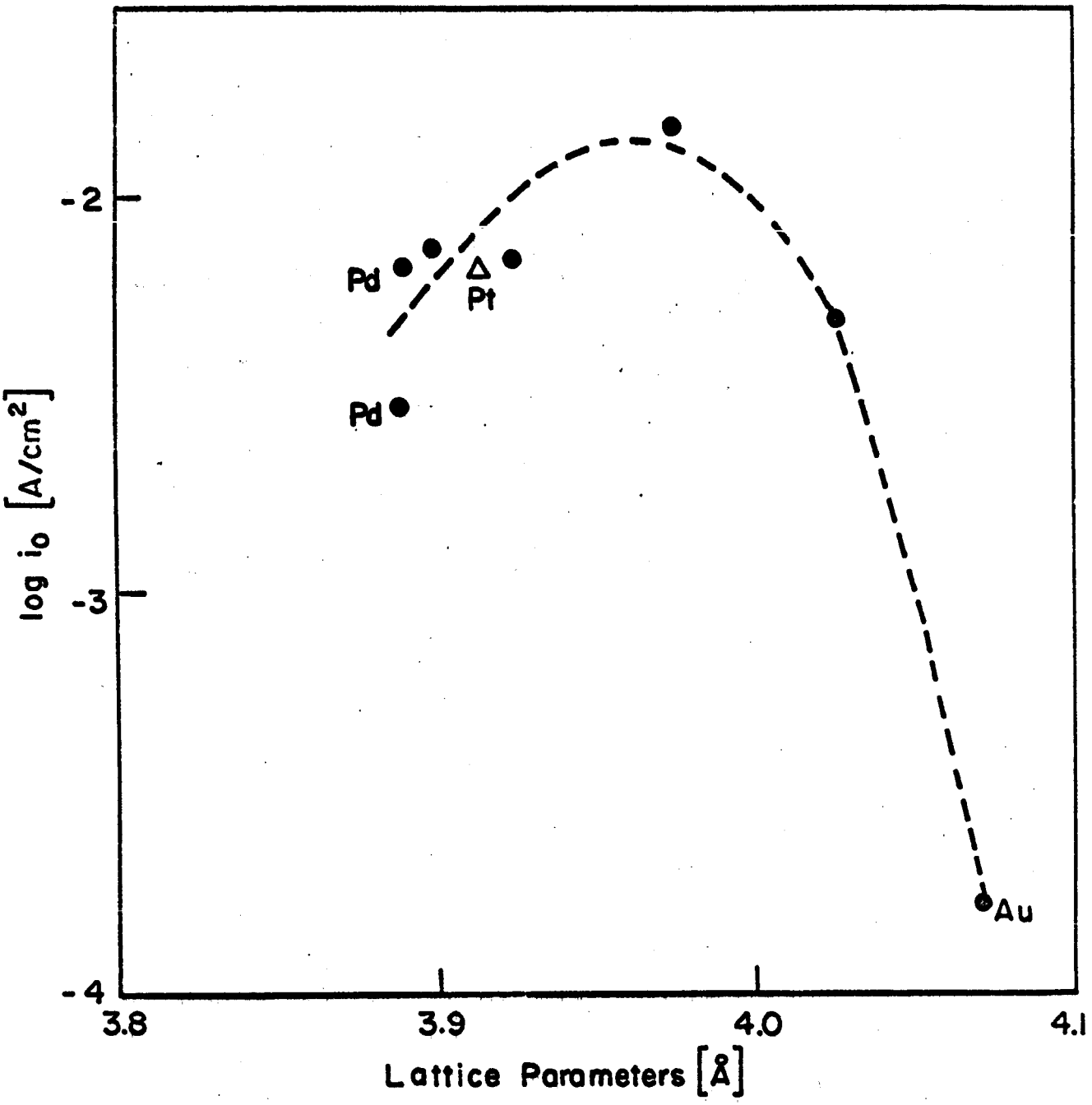

FIG.2

Exchange current density for Fe^{2+}/Fe^{3+} reaction vs lattice parameters of Pd-Au alloys. Pt is included.

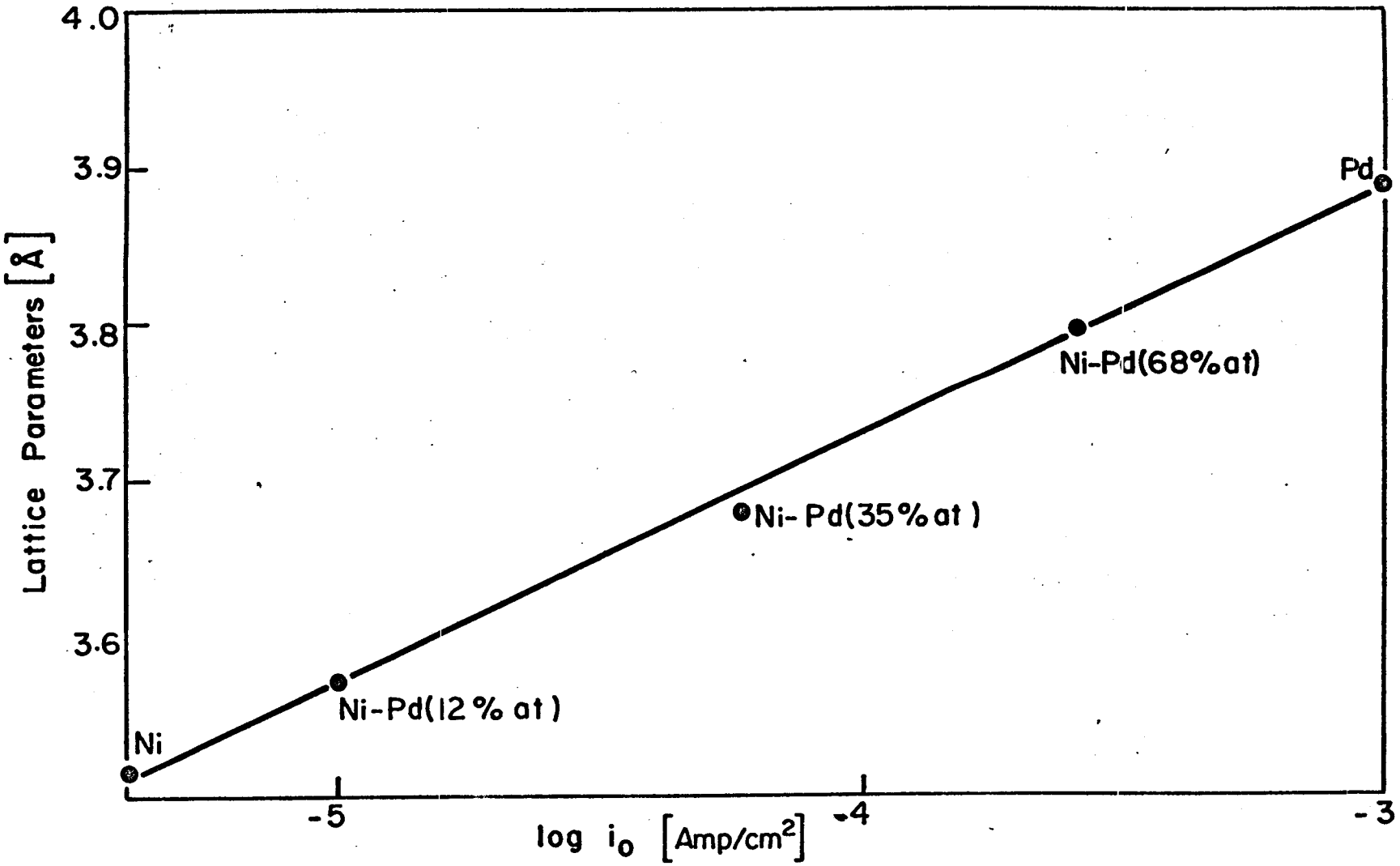

FIG.3

Exchange current density for H_2/H^+ reaction vs lattice parameters of Ni-Pd alloys.

III. THE ELECTRICAL DOUBLE LAYER AT THE SOLID-SOLUTION INTERFACE

In the quarterly report period capacitance behavior of gold electrodes was studied as a function of electrode potential and frequency.

1. Experimental

The apparatus used is described in a previous report [1]. It consisted of a transformer ratio arm bridge, 302A Hewlett-Packard wave analyzer and a Tektronix oscilloscope.

The electrode material used was Johnson Matthew 'Grade 1' gold. The gold wire (7 cm) was spot-welded to a thin platinum foil (1 cm x 0.2 cm) to the other end of which a small length (2 cm) of platinum wire was attached. The gold wire was put in a small capillary attached to a $\sim$30" piece of 'trubore' tubing and was sealed with pyrex glass under vacuum. The platinum foil formed a vacuum-tight seal with glass after being heated strongly. If vacuum sealing of gold to glass was not adopted, the wire was observed to melt inside the thin walled glass capillary. The glass capillary was broken off at the requisite position. The glass tubing with the wire was cleaned with ispropyl alcohol, distilled water and was kept in HNO_3-H_2SO_4 for several hours. It was rinsed with distilled water and conductivity water several times. The wire was melted into a fine spherical ball with an oxy-hydrogen flame. The electrode was immediately transferred into a furnace made to fit on top of the conventional electrolytic cell. The electrode was heated in argon for 1/2 - 1 hour to remove the mositure, and in hydrogen

for 10 - 20 minutes at 350°C and in argon at about 400°C for another hour or so. The electrode was cooled in the same atmosphere and slid directly (without exposing to outside environment) into the main compartment. It was surrounded by a platinized platinum spherical basket which served as the counter electrode.

The solutions were prepared from analyzed reagent grade perchloric acid and sodium hydroxide and recrystallized sodium perchlorate and redistilled conductivity water which was distilled directly into the pre-electrolysis cell under purified nitrogen atmosphere. Solutions were pre-electrolyzed between large platinized platinum gauze (150 cm^2 geo) electrodes, for at least 24 hours and maximum of 72 hours.

2. Results

Figure 1 shows the typical variation of capacitance with potential on gold in 10^{-3} N perchloric acid. There is no hysteresis in capacitance, if the potential of the electrode is not made more than 200 mv positive or negative to the potential of zero charge. If the electrode is taken to 1000 mv (r.h.e.) and the readings taken while making the potential more anodic and then coming back in potential, considerable hysteresis is seen to occur (Fig. 2). From Fig. 3, it can be observed that giving an anodic and cathodic pulse does not change the position of potential of zero charge.

Fig. 4 shows the effect of frequency on capacitance as a function of potential.

It can be seen that the capacitance does not change considerably

as a function of frequency. The potential of zero charge is independent of frequency. The slight dependence of capacitance on frequency may be explained by the imperfections on the metal surface.

It was observed that the potential of zero charge in acidic solutions did not depend on pH. But in alkaline solutions we were unable to obtain capacitance curves similar to those in acidic solutions with same ionic strength. Whereas reducing the ionic strength, i.e. no addition of sodium perchlorate and very dilute sodium hydroxide solutions (pH $\sim$ 9) gave similar curves. The potential of zero charge was found to be about + 10 mv (N.H.E.) as compared to + 170 mv (N.H.E.) at pH 3.0. The shift of p.z.c. could be due to a combined effect of OH^- adsorption and reduction of ionic strength of the solutions.

3. Future Work

Potential of zero charge on silver and nickel will be studied. Also, apparatus will be designed and built for the measurement of the potential of zero charge by a third independent method.

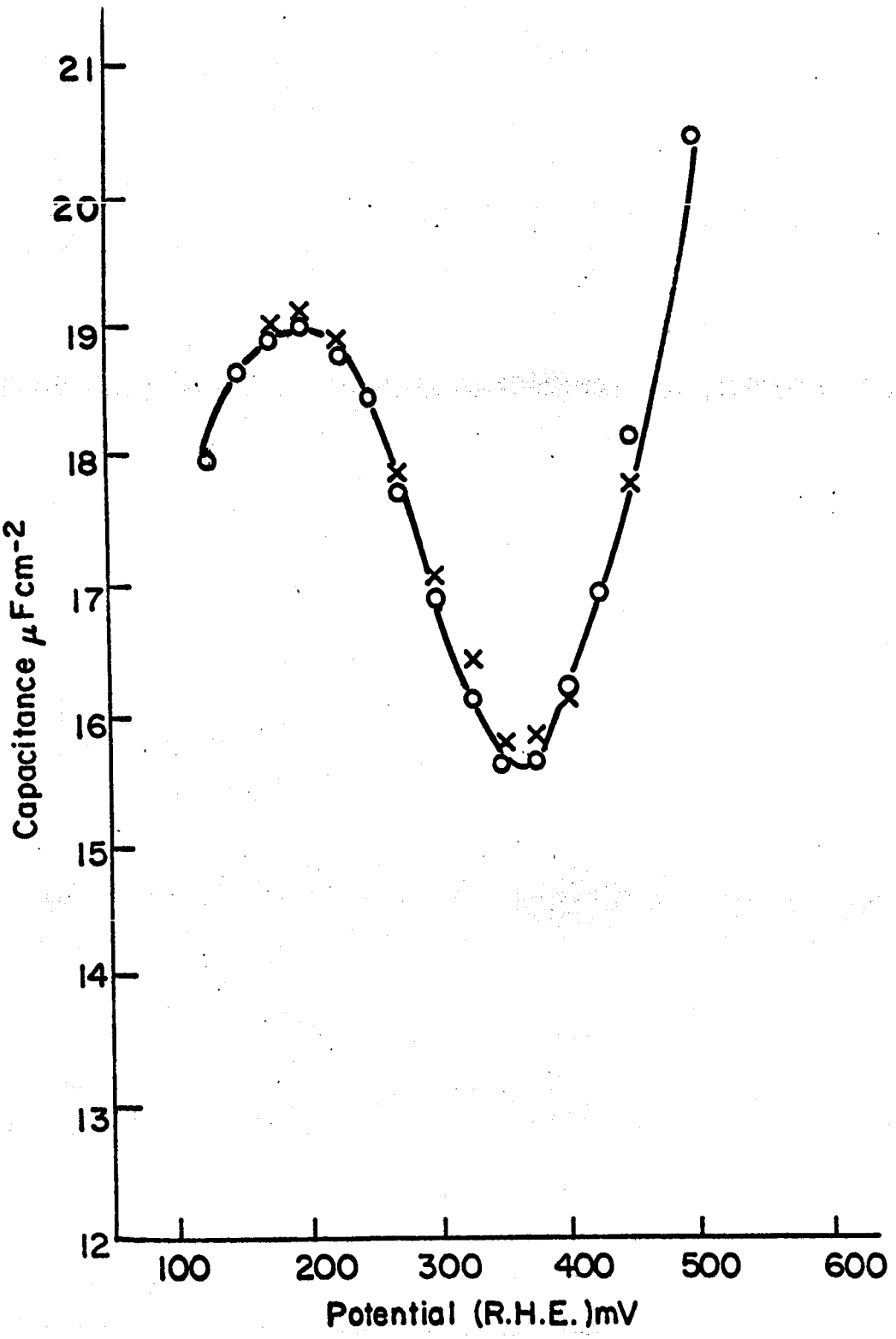
21
20
19
18
17
16
15
14
13
12
Capacitance μFcm⁻²
100
200
300
400
500
600
Potential (R.H.E.)mV

FIG.1

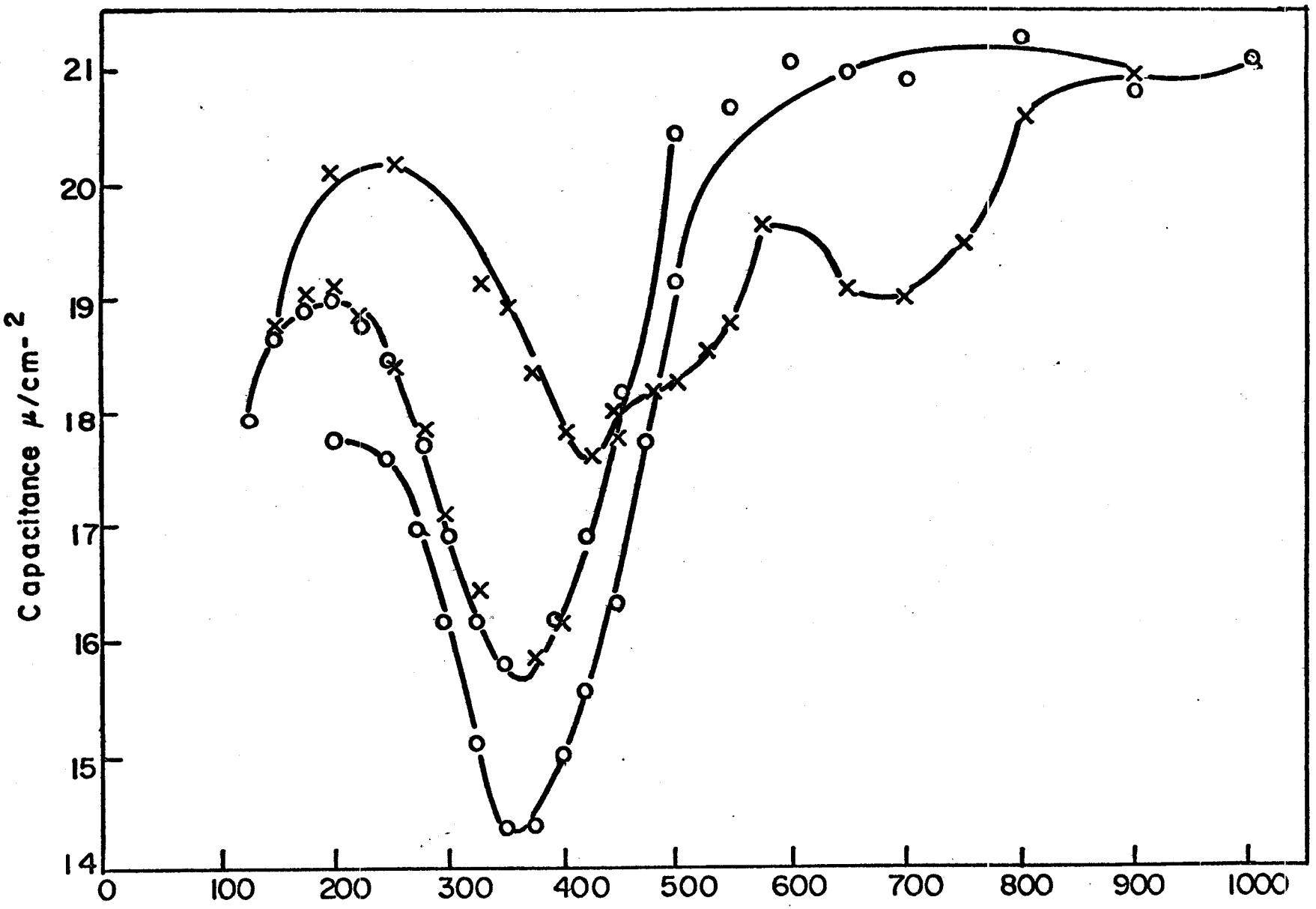
Capacitance μ/cm⁻²
21
20
19
18
17
16
15
14
0
100
200
300
400
500
600
700
800
900
1000

FIG.2

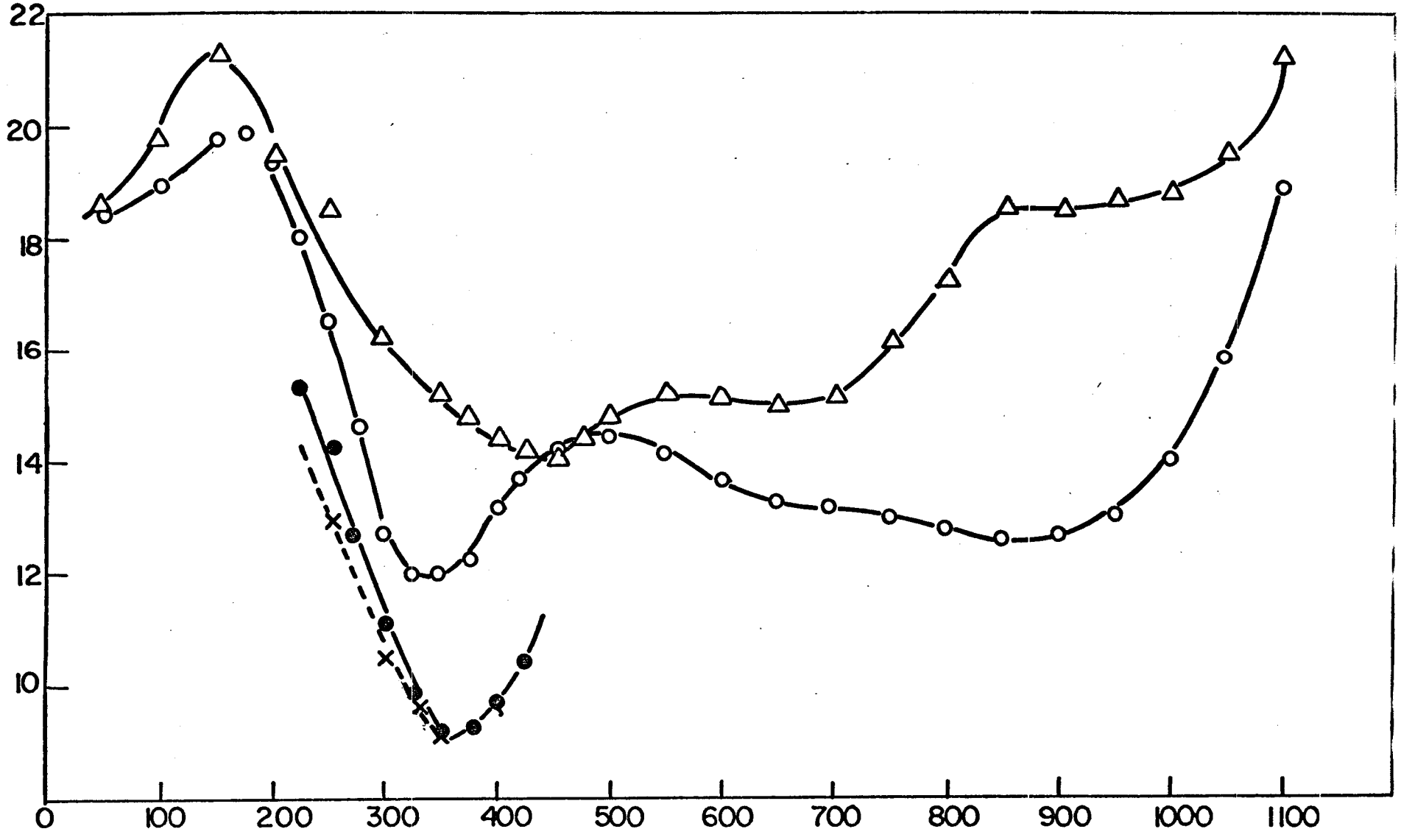
22
20
18
16
14
12
10
0
100
200
300
400
500
600
700
800
900
1000
1100

FIG. 3

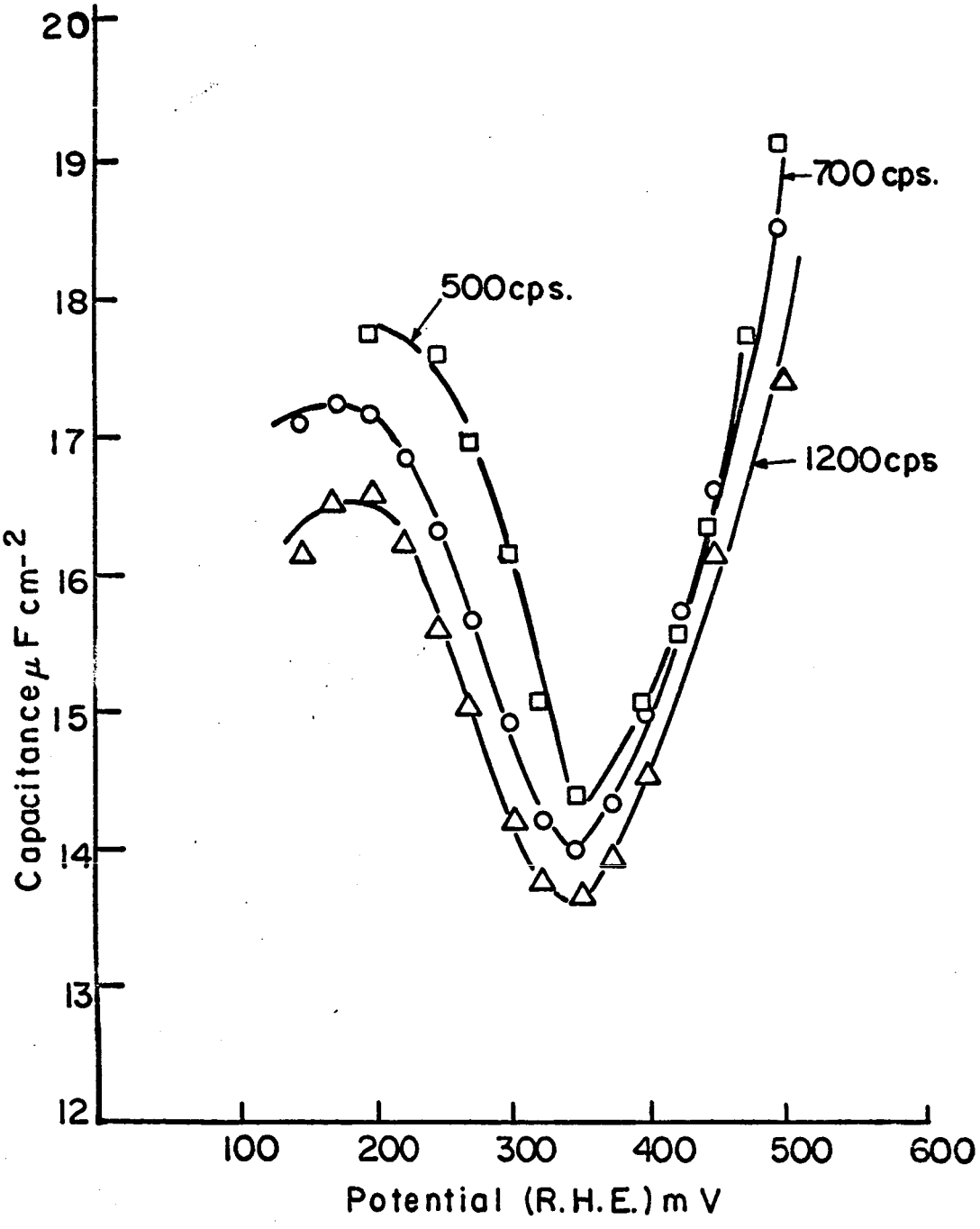
20
19
18
17
16
15
14
13
12
Capacitance μ F cm-2
700 cps.
500cps.
1200cps
100
200
300
400
500
600
Potential (R.H.E.) m V

FIG. 4

IV. ADSORPTION IN THE DOUBLE LAYER WITH SPECIFIC REFERENCE TO THERMAL EFFECTS

1. Introduction

In view of the importance of adsorption measurements for determination of mechanism and understanding of electrocatalysis in fuel cell systems, the methods of adsorption measurements must be critically evaluated. In recent years the potential sweep method gained a great deal of attention, since it is a relatively quick and easy way of obtaining extremely well reproducible current-potential transients. The interpretation of these transients, however, raises serious doubts.[1]

In order to check the validity of implicit assumptions contained in the method, a comparison was made of the results obtained by a previously developed radioactive technique[2,3] and by the potential sweep, in two systems: benzene and ethylene dissolved in 1 N H_2SO_4.

2. Experimental

2.1 Potential-sweep Method

Platinized Pt bead serves as the potentiostated anode. Its surface area is derived from capacity measurements in the double layer region in blank solution (saturated with N_2), assuming a capacity of $20\,\mu F\ cm^{-2}$. The electrode is prepared before each potential sweep in the way similar to that proposed by Niedrach,[4] i.e. it is potentiostated for

(A) 10 secs at 1.7 V

(B) 20 secs at 1.2 V

(C) 15 secs at 0.06 V

(A) - adsorption step in which the electrode is held for the desired amount of time (t_A) at the adsorption potential (V_A). After the period t_A a potential sweep is applied with a constant rate dV/dt, reversing the direction at the potential where O_2 evolution starts ($\sim$1.6 - 1.7 V) and returning back to V_{ad} (see Fig. 1 Curve 1). The same potential sweep, under identical conditions is previously carried out in a blank solution (Fig. 1 Curve 2). The difference in the areas of the anodic current (i.e. above the 0 line in Fig. 1) is then assumed to be the amount of coulombs used to burn off the adsorbed fuel.

2.2 Radiotracer Method

This was described in detail in Report No. 1 (1 Oct. 1962 - 31 March 1963).

3. Results

3.1 Determination of the useful sweep rate

Preliminary measurements with different sweep rates have been done, for both systems: with benzene (7×10^{-6} M/l), and with ethylene (4×10^{-5} M/l). The range between 0.1 and 1000 V/sec has been explored. Fig. 2 shows dependence of coul/cm^2 on different sweep rates. The plateau is achieved between 0.3 and 1 V/sec for ethylene adsorption, and between 0.1 and 2 V/sec for benzene. Therefore the sweep rates used in subsequent experiments were 0.5 V/sec for ethylene and 0.2 V/sec for benzene.

Above the range of sweep rates in which the plateau is achieved, Q decreases becoming negative at high sweep rates ($\Delta V/\Delta t > 100$ V/sec).

Below this range higher values of Q obtained may be interpreted as readsorption of ethylene and benzene, respectively, during the sweep.

3.2 Time dependence of adsorption

This is shown in Fig. 3: curve 1, benzene; curve 2, ethylene. For both systems after $t_A = 5$ min no significant change is shown by potential sweep method. In view of these results $t_A = 5$ min was used in determination of potential dependence of adsorption.

3.3 Potential dependence of adsorption

Fig. 4 (circles) represents the results obtained in investigated potential region (from 100 - 800 mV); for benzene and Fig. 5 for ethylene. Results obtained by radiotracer measurements are shown in both Figures (triangles).

4. Discussion

The preliminary results obtained here do not allow yet to draw conclusions as to the validity of the sweep method. There are large differences in the time dependence of adsorption as measured by the two methods: potential sweep indicating steady state after 3 - 5 min, whereas the radiotracer method shows marked time dependence up to 30 min. The shape of the Θ - V curve in the case of ethylene is different (cf. Fig. 5). On the other hand the results of potential dependence of

benzene adsorption (Fig. 4) agree remarkably well. The agreement in the latter case is better than that expected when taking into account experimental errors.

5. Future Work

Further and more detailed comparison will be made between both methods by obtaining the adsorption isotherms at a few potentials for benzene and ethylene.

Adsorption of naphthalene and n-decylamine will be investigated by means of potential sweep method and compared with radiotracer results obtained previously.[5,6]

References

1. Three-quarter Progress Report (1 Oct. 1965 to 30 June 1965). (APPENDIX II).
2. E. Gileadi, B. T. Rubin and J. O'M. Bockris, J. Phys. Chem., 69, 3335 (1965).
3. W. Heiland, E. Gileadi and J. O'M. Bockris, in process of publication.
4. L. W. Niedrach, S. Gilman and I. Weistock, J. Electrochem. Soc., 112, 1161 (1965).
5. J. O'M. Bockris and D. A. J. Swinkels, J. Electrochem. Soc., 111, 756 (1966).
6. J. O'M. Bockris, M. Green and D. A. J. Swinkels, J. Electrochem. Soc., 111, 743 (1964).

CAPTIONS TO FIGURES

Figure 1. Typical i - V transient --- blank; —— with ethylene.

Figure 2. Dependence of charge on sweep rate, for ethylene in 1 N H_2SO_4 at 30°C. (Conc. of ethylene 4 x 10^{-5} mole/l).

Figure 3. Dependence of adsorption on time in 1 N H_2SO_4 at V = 0.3 V vs. N.H.E. Curve 1, 1a: benzene (7 x 10^{-6} mole/l; t = 50°C) Curve 2, 2a: ethylene (4 x 10^{-5} mole/l; t = 30°C) 1,2 - potential sweep method; 1a, 2a - radiotracer method.

Figure 4. Coverage-potential relatinnship for benzene in 1 N H_2SO_4 at 50°C. Concentration of benzene 7 x 10^{-6} mole/l. ... potential sweep method; △△△ radiotracer method.

Figure 5. Surface excess-potential relationship for ethylene in 1 N H_2SO_4 at 30°C. Concentration of ethylene 4 x 10^{-5} mole/l. ... potential sweep method; △△△ radiotracer method.

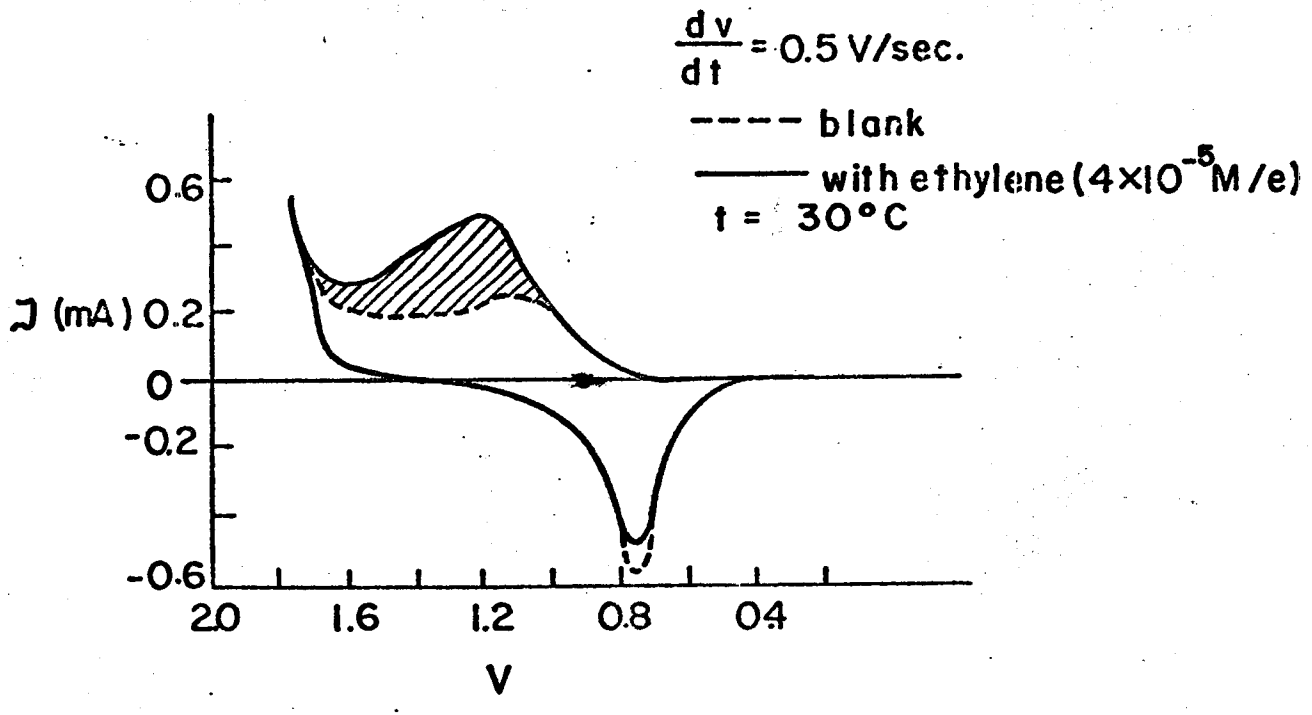
dv/dt = 0.5 V/sec.
---- blank
—— with ethylene (4×10⁻⁵ M/e)
t = 30°C
0.6
J (mA) 0.2
0
-0.2
-0.6
2.0
1.6
1.2
0.8
04
V

FIG. 1

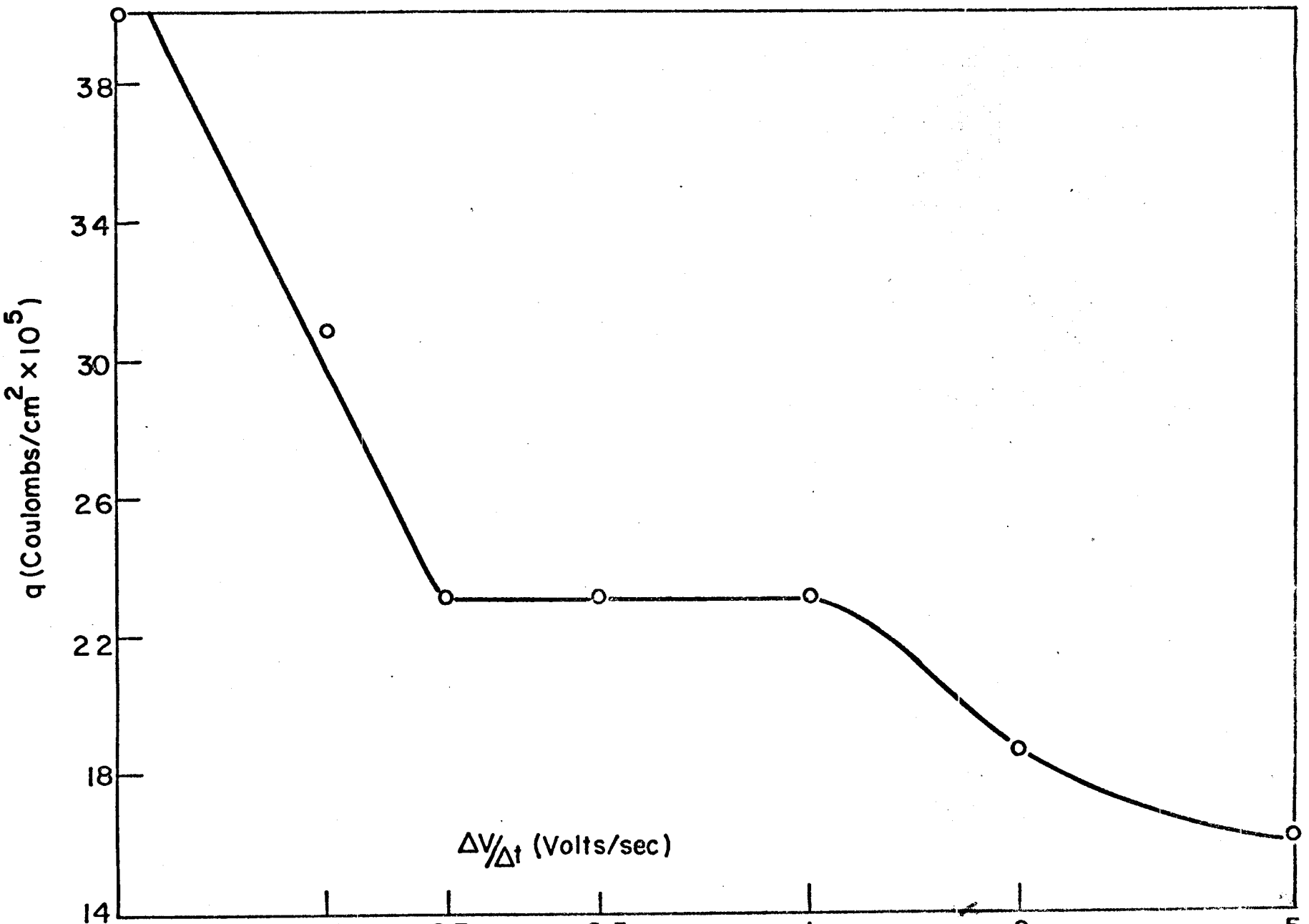
38
34
30
26
22
18
14
q (Coulombs/cm^2 x 10^5)
0.2
0.3
0.5
1
2
5
$\Delta V/\Delta t$ (Volts/sec)

FIG.2

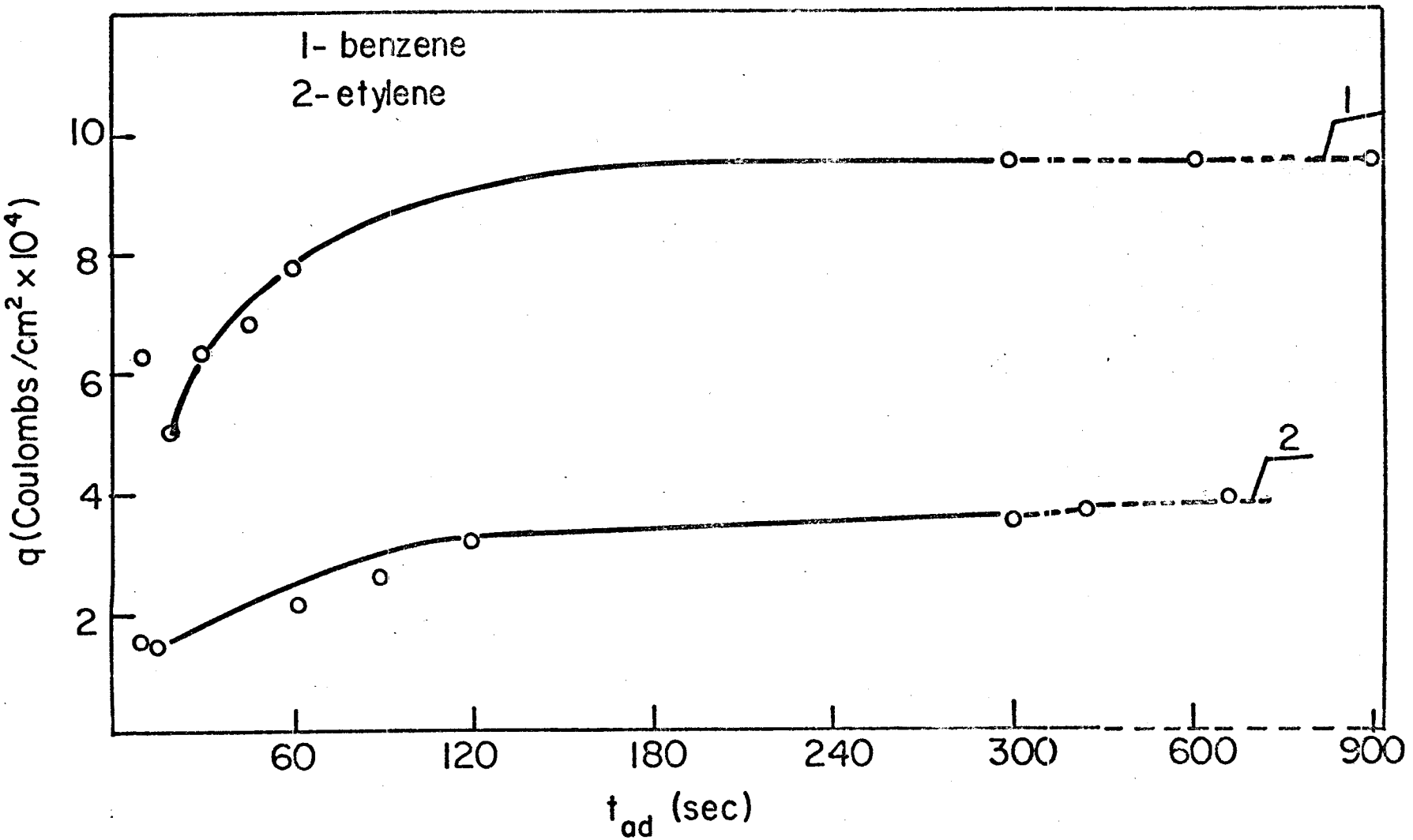
1- benzene
2- etylene
1
2
10
8
6
4
2
60
120
180
240
300
600
900
q (Coulombs /cm² x 10⁴)
t_ad (sec)

FIG. 3

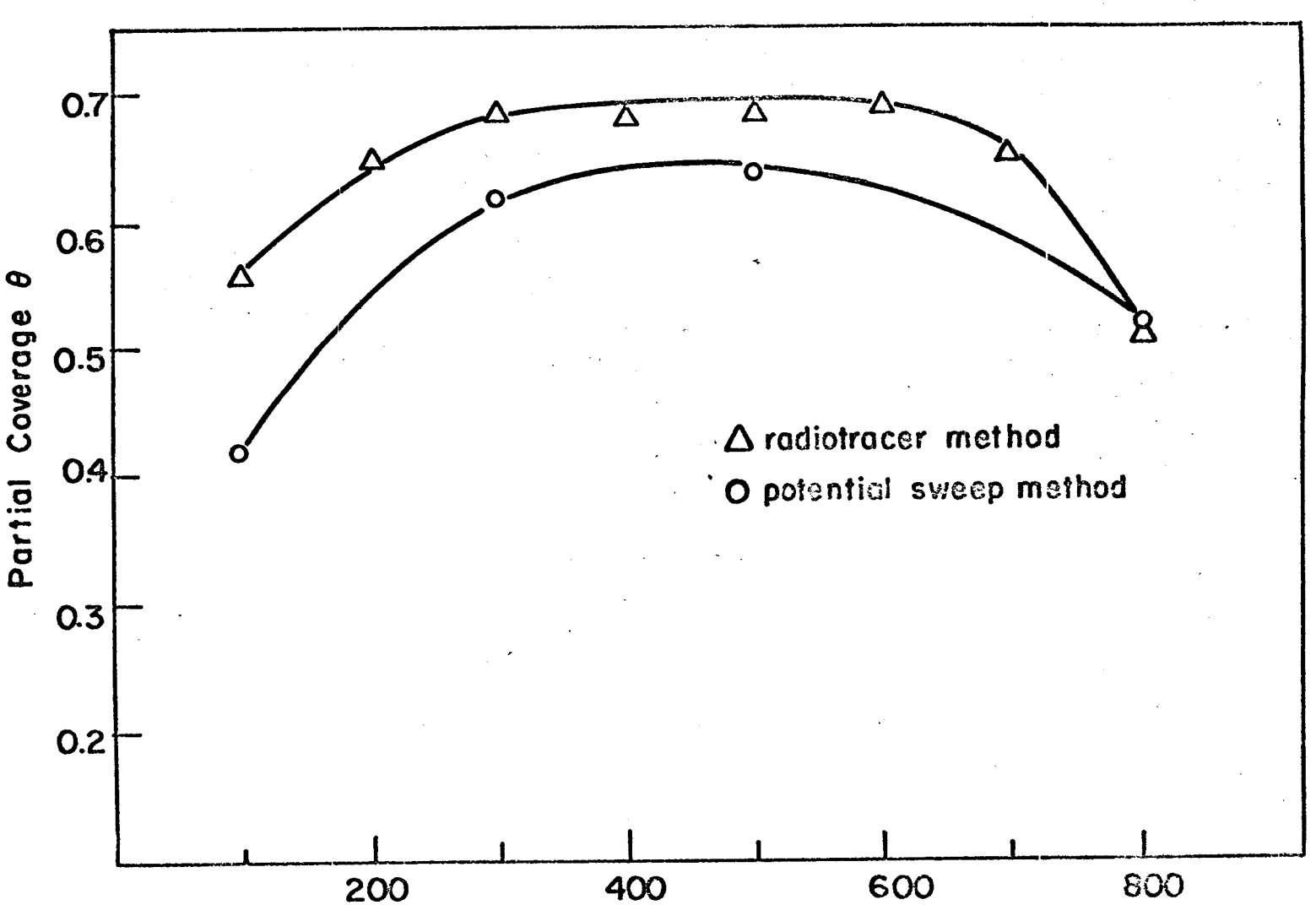
0.7
0.6
0.5
0.4
0.3
0.2
Partial Coverage θ
200
400
600
800
Potential (mV vs.N.H.E.)
△ radiotracer method
O potential sweep method

FIG.4

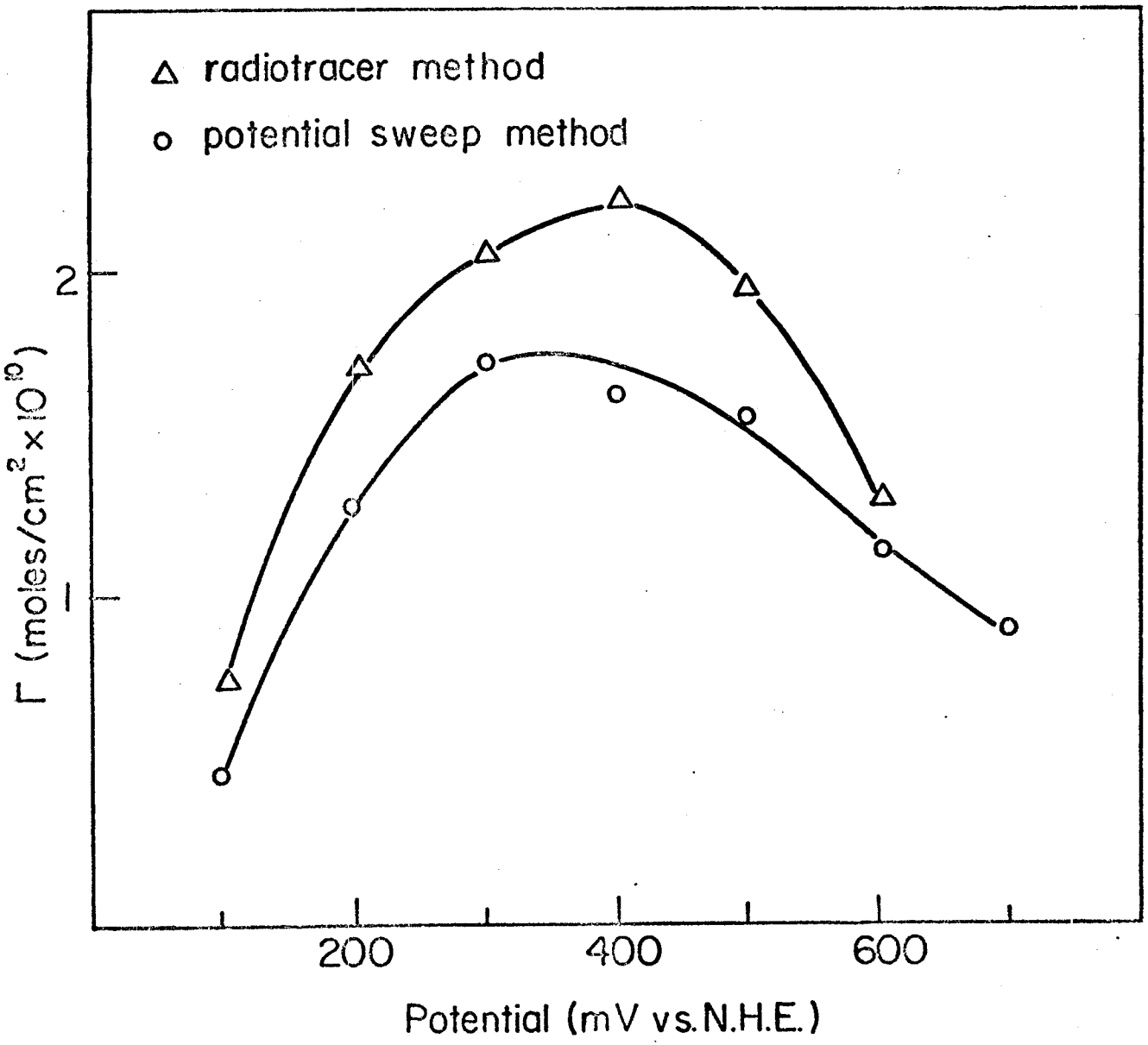
△ radiotracer method
o potential sweep method
Γ (moles/cm² x 10¹⁰)
2
1
200
400
600
Potential (mV vs. N.H.E.)

FIG. 5

V. ELECTRODE KINETIC ASPECTS OF ELECTROCHEMICAL ENERGY CONVERSION

THE KINETICS OF REACTIONS AT POROUS ELECTRODES

This work was carried out in collaboration with Dr. H. Hurwitz

A. The Simple Pore Model

1. General

The structures of porous electrodes are quite complex. For the purpose of simplifying the mathematical treatment, the electrodes are assumed to consist of uniform parallel cylindrical pores of some average radius. Thus, one can analyze the current-potential relation in a single pore and then radii from the number of pores per cm^2 of cross section of the porous electrode, obtain the current density-overpotential relation of the reaction at the porous electrode.

Another useful relationship is the current distribution within the porous electrode. This is obtained from the analysis of the single pore.

For this purpose, two models -- the simple pore model and the thin film model -- are chosen.(Fig. 17). These models represent in a way the extreme types of the modes of operations which correspond to non-wetting and wetting electrodes. The simple pore model is analyzed in the present report.

2. Reaction Scheme

A reaction is considered to occur in the following consecutive steps:

$$R_{gas} \longrightarrow R_{sol,b} \tag{1}$$

$$R_{sol,b} \longrightarrow R_{sol,e} \tag{2}$$

$$R_{sol,e} \longrightarrow R_{ads} \tag{3}$$

$$R_{ads} \longrightarrow R^{+}_{ads} + e_o^{-} \tag{4}$$

$$R^{+}_{ads} \longrightarrow P + (n-1)\ e_o^{-} \tag{5}$$

R represents a gaseous reactant and P the products. The suffices b and e stand for the gas-electrolyte boundary (vide models below) and the electrode-electrolyte interface. It is assumed that equation (4) represents the activation controlled step at the electrode. All steps grouped together under equation (5) are assumed to be fast. As examples of this type of reaction one may consider the hydrogen dissolution reaction or oxidation of saturated hydrocarbons. A corresponding cathodic reaction is that of oxygen reduction.

3. Description of simple pore model

A single pore of the electrode is represented in Fig. 1. A cylindrical coordinate system is used. For simplicity, it is assumed that the meniscus at the gas-electrolyte interface at z = 0 is flat. The reactant gas diffuses through the pore to the gas-electrolyte interface at z = 0, where it dissolves in the electrolyte and the dissolved gas diffuses through the electrolyte to the various electrocatalytic sites along the pore at which the reaction occurs. In the following treatment, it is assumed that the first and second steps of diffusion

of reactant gas through the electrolyte free part of the pore ($z < 0$) and of dissolution of the gas at the gas-electrolyte interface are fast. The other steps of the reaction are represented by equations (1) to (5).

3. Theoretical analysis of model:

(i) Case where all forms of polarization are taken into account

A rigorous analysis of the current-potential relation and current distribution in a single pore is a two-dimensional problem (due to cylindrical symmetry). However, it is not possible to solve this two-dimensional problem taking into account all forms of polarization. Thus, the present analysis was carried out considering a concentration gradient of reactant in one direction -- the axial direction of the pore. The assumption of a unidirectional concentration gradient is valid under the conditions that the local activation controlled current density is less than the limiting current density due to radial diffusion. Expressed mathematically this condition is

$$i_o \exp(\beta \eta F/RT) << DnFc^o/r_2 \qquad (6)$$

Further, the one-dimensional model is valid for currents up to about 10% of the limiting current density in the pore (the validity of this assumption is confirmed by considering the two-dimensional treatment for the case of activation and concentration polarization, details of which will appear in a forthcoming publication).

The basic equations for the one-dimensional model are obtained by considering a cylindrical element of thickness dz (Fig. 1).

The current generated in this element (dI) is given by

$$dI = 2\pi r_2 \, dz \, i_o \left[(c_z/c^o) \exp(\beta \eta F/RT) - \exp\left\{-(1-\beta)\eta F/RT\right\}\right] \tag{7}$$

where i_o is the exchange current density for the reaction, c_z is the concentration at the electrode-electrolyte interface between z = z and z = z + dz and η is the overpotential at z = z.

The ohmic drop in the element dz is given by

$$d\eta = I(dz/\kappa \pi r_2^2) \tag{8}$$

where κ is the specific conductivity of the electrolyte and I is the total current generated from z = 0 to z = z.

The third important relation is obtained by using the stationary state hypothesis for the reactant R in the element dz. Thus,

$$dI/dz = \pi r_2^2 \, DnF \, (d^2c_z/dz^2) \tag{9}$$

where D is the diffusion coefficient of the reactant in the electrolyte.

The boundary conditions for this problem are

$$\eta = \eta_o \text{ at } z = 0 \tag{10}$$

$$I = \kappa \pi r_2^2 (\partial \eta/\partial z) = 0 \text{ at } z = 0 \tag{11}$$

$$c = c^o \text{ at } z = 0 \tag{12}$$

$$\pi r_2^2 \, DnF(\partial c/\partial z) = -I_t \text{ at } z = 0 \tag{13}$$

and

$$dc/dz = 0 \text{ at } z = 1 \tag{14}$$

The derivation of the solution of the differential equations (7) to (9) with boundary conditions (10) to (14) is rather involved. The

current, I, is expressed as a function of the distance by the relation

$$I = (2\pi r_2^2 RT)/\ell F \left[\left\{ ab \exp(y_o) \right\}^{1/2} \exp(mx/2)(dc/d\alpha) + m \right] \quad (15)$$

where

$$a = i_o \ell^2 F/\pi r_2 RT \quad (16)$$

$$b = DnF^2 c^o/2KRT \quad (17)$$

$$y_o = \eta_o F/2RT \quad (\beta \text{ assumed to be half}) \quad (18)$$

$$m = \ell F I_t/2\pi r_2^2 KRT \quad (19)$$

$$\alpha = 2\left[a \exp(y_o + mx)/bm^2 \right]^{1/2} \quad (20)$$

$$x = z/\ell \quad (21)$$

and $$dc/d\alpha = \left[1-\exp(-2y_o)\right] \frac{K_1(\alpha_2)I_1(\alpha) - I_1(\alpha_2) K_1(\alpha)}{K_o(\alpha_1)I_1(\alpha_2) + I_o(\alpha_1)K_1(\alpha_2)} \quad (22)$$

α_1 and α_2 are the values of α evaluated at x = 0 and x = 1 respectively.

Use of the possible numerical values of the constants of the above equations in equations (15) and (22) shows that α is always large. Under these conditions, the equation for I reduces to

$$I_z/I_t = (\sinh K - \sinh K(1-x))/\sinh K \quad (23)$$

where

$$I_t = \frac{\pi r_2^2 DnFc^o K}{\ell} \left[1 - \exp(-2y_o)\right] \tanh K \quad (24)$$

and $$K = (a/b)^{1/2} \exp(y_o/2) \quad (25)$$

This limiting case corresponds to one of only activation and coneentration

polarization in the pore.

Two limiting cases may be considered: when K is small,

$$\tanh K \simeq K \tag{26}$$

$$\sinh K \simeq K \tag{27}$$

$$\sinh K(1 - x) \simeq K(1 - x) \tag{28}$$

Thus, equations (23) and (24) become

$$I_z/I_t = x \tag{29}$$

and

$$I_t = (\pi r_2^2 DnFc^o K^2)/\ell \left[1 - \exp(-2y_o) \right] \tag{30}$$

Using K^2 as given by equations (16) to (18) and (25) in (30), it follows that the Tafel slope is 2RT/F and from (29) that there is a uniform current distribution in the pore. This case corresponds to one of low i_o, high $DnFc^o$ and low η_o.

The second case is when K is large. Under these conditions,

$$\tanh K \simeq 1 \tag{31}$$

$$\sinh K \simeq 1/2 \exp K \tag{32}$$

$$\sinh K(1 - x) \simeq 1/2 \exp K\,(1 - x) \tag{33}$$

Using equations (31) to (33) in equations (23) and (24)

$$I_z/I_t = \left[1 - \exp(-Kx) \right] \tag{34}$$

and

$$I_t = (\pi r_2^2 DnFc^o)/\ell\, K \left[1 - \exp(-2y_o) \right] \tag{35}$$

In this case, the Tafel slope is 4RT/F and is obtained for the case when i_o is high, $DnFc^o$ is low or η_o is high.

However, in both cases, the exchange current density influences the total current generated in the pore. In the first case, I_t varies linearly with i_o whereas in the second, I_t varies linearly with $(i_o)^{1/2}$. In the former case, the normal Tafel slope as for a planar electrode is obtained, whereas in the latter, twice the normal Tafel is obtained. Thus, it is quite clear that the use of porous electrodes alone does not eliminate the problem of electrocatalysis.

Figure 3 shows the overpotential-current relation in a single pore for two values of i_o (10^{-12}, 10^{-9} and 10^{-6} amp cm^{-2}). Using the same values of $DnFc^o$, the effect of the exchange current density on the relations is clearly seen. Fig. 3 illustrates the effect of variation of the parameter K on the current distribution within the electrode. Plots in terms of the parameter K are quite convenient since from a few plots one may predict the nature of the curves for variations in i_o, η_o, D, c^o and r.

(ii) Case where only activation and concentration polarization are present

As seen from the preceding section, for the most probable values of $DnFc^o$, the ohmic drop in the pore is insignificant. Thus, from the general case of all forms of polarization, equations were obtained for the limiting case of activation and concentration polarization using a one-dimensional treatment. It is possible to carry out a two-dimensional treatment for the case of only activation and concentration polarization from analogous problems in heat transfer. A comparison of the one and two-dimensional treatments was made and it was found that for high

values of the ratio ℓ/r_2, the current-potential behavior in both are identical up to about 10% of the limiting current. Above this value of the current, only the two-dimensional treatment is valid.

(iii) Case where only activation and ohmic polarization are present

This case is applicable when the product $DnFc^o$ is quite high, e.g., Cl_2 in aqueous solution or if liquid fuels soluble in the electrolyte such as methanol are used. Another example is if the reactant saturated electrolyte is circulated through the pore at a rate such that there is no concentration gradient in the pore. The basic equations necessary for solving this problem are equations (7) (with $c_e = c^o$) and (8). Two cases may be distinguished. When $\eta_o < 0.1$ V,

$$I_z/I_t = \frac{(\tan(\psi)_{x=x}}{(\tan(\psi)_{x=0}}$$

and $$I_t = 4K\pi r_2^2(RT/F)(zi_oF/Kr_2RT)\sinh(y_o/2)\ \tan(\psi)_{x=0} \qquad (37)$$

where $$F(k,\psi) = \int_o^{\psi} d\psi/(1 - k^2 \sin^2\psi)^{1/2} \qquad (38)$$

with $$k = 1/\cosh(y_o/2) \qquad (39)$$

and $$\cos\psi = \sinh(y_o/2)/\sinh(y/2) \qquad (40)$$

When $\eta_o > 0.1$ V, the rate of the reverse step is so small in comparison with the forward rate that it may be neglected. Under these conditions

$$I_z/I_t = \tan Ax/\tan A \qquad (41)$$

and $$I_t = \left[(4RT/\ell F)K\pi r_2^2\right] A \tan A \qquad (42)$$

where $$A = (i_o \ell^2 F/2\kappa r_2 RT)^{1/2} \exp y_o/2 \qquad (43)$$

The relations (41) and (42) present in a simplified manner the effect of variation of the parameters i_o, r_2, K, ℓ, η_o by considering only changes in the parameter A. A has to be less than $\pi/2$; when A = $\pi/2$, the current at $z = \ell$ is ∞. Figures 4 and 5 show the variation of I_z/I_t and of $(\eta - \eta_o)$ vs z for different values of one of the above parameters, keeping the others constant. For an i_o of 10^{-3} amp cm^{-2}, with κ = 1 ohm^{-1} cm^{-1} and $r_2 = 10^{-4}$ cm, and $\ell = 10^{-1}$ cm, the behavior corresponding to A = 1.55 is observed only at η_ℓ = 0.4 V. Using the same values of $\kappa_1 r_2$ and l, but $i_o = 10^{-6}$ amp cm^{-2}, the same current distribution is obtained for η_ℓ = 0.74 V and with $i_o = 10^{-9}$ amp cm^{-2} at η_o = 1.09 V.

Using this parameter A, the current-potential relation in the pore may also be easily obtained. Such plots for $i_o = 10^{-6}$ and 10^{-9} amp cm^{-2} are shown in Fig. 6 illustrating the electrocatalytic effect of the substrate on the current obtainable from a porous electrode. It is interesting to note that the current densities observed in this case are many orders of magnitude (about 10^3 times) than for the corresponding case of activation and concentration polarization.

Captions to Figures

1. The simple pore and thin film models.

2. Overpotential-current density relation for case where all forms of polarization are considered. Assumed parameters: $DnFc^{o}$ - 10^{-7} amp cm^{-1}, ✕ = 1 ohm^{-1} cm^{-1}; 0 - $i_o = 10^{-12}$ amp cm^{-2}; □ - 10^{-9} amp cm^{-2}; △ - 10^{-6} amp cm^{-2}.

3. Current distribution relations for case where all forms of polarization are considered. Values of $DnFc^{o}$ and ✕ as in (2).
   (a) Uniform current distribution in the pore, e.g., with i_o = 10^{-12} amp cm^{-2} and η = 0.1 V.
   (b) $i_o = 10^{-9}$ amp cm^{-2} and η = 0.1 V
   (c) $i_o = 10^{-12}$ amp cm^{-2} and η = 0.65 V
   or $i_o = 10^{-12}$ amp cm^{-2} and η = 0.01 V
   (d) $i_o = 10^{-9}$ amp cm^{-2} and η = 0.65 V.

4. Current distribution relations as a function of parameter A for case of activation and ohmic polarization. A values are for ⊠ 0.50; ⊕ 0.60; ● 0.70; △ 0.80; ▽ 0.90; 0 1.00; □ 1.10; △ 1.20; ▽ 1.30; X 1.40; + 1.45; 0 1.50; ■ - 1.55.

5. Potential distribution relations as a function of parameter A for case of activation and ohmic polarization. Symbols for A values same as for figure 4.

6. Overpotential-current density relation for case of activation and ohmic polarization. ✕ = 1 ohm^{-1} cm^{-1}; (a) $i_o = 10^{-9}$ amp cm^{-2}, (b) $i_o = 10^{-6}$ amp cm^{-2}.

Simple Pore Model

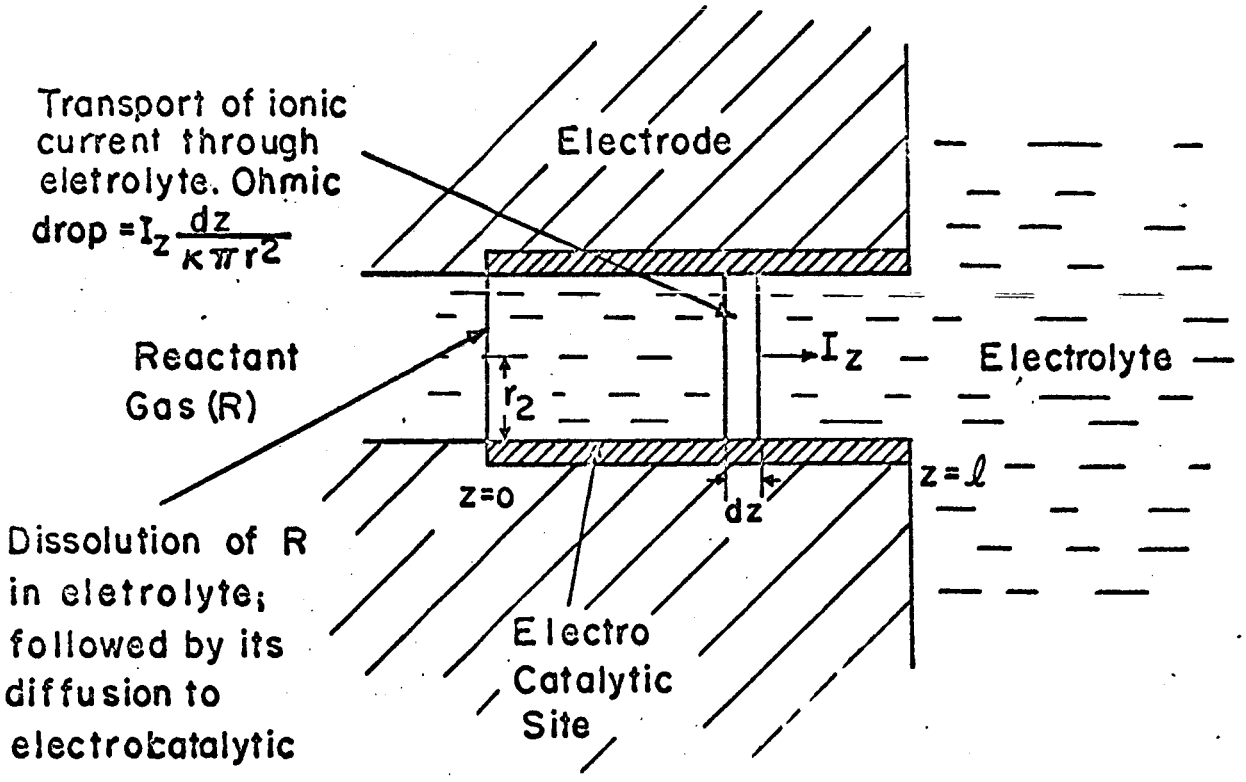

Thin Film Model

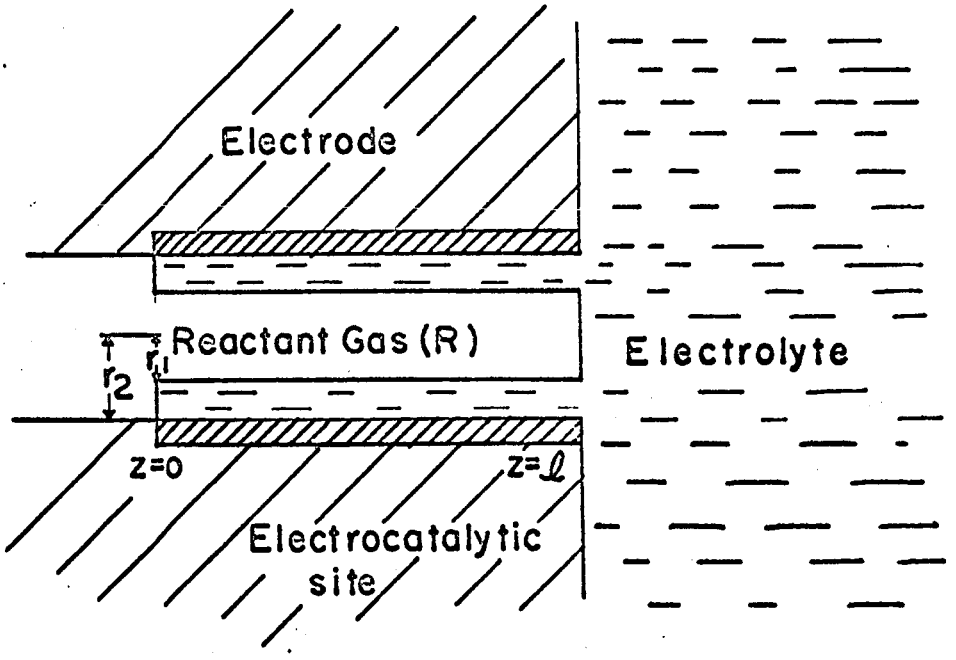

FIG.1

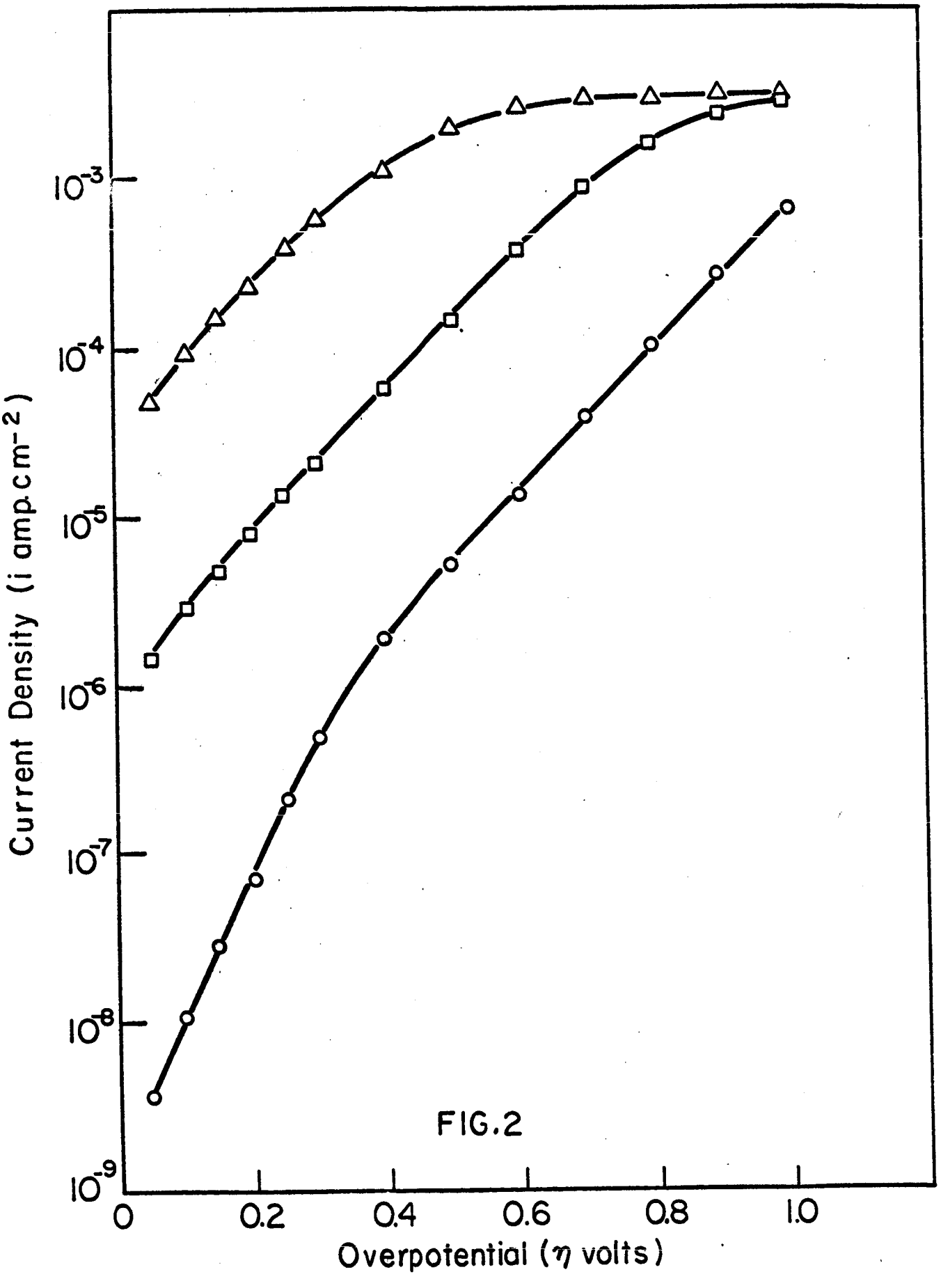
Current Density (i amp.cm^{-2})
10^{-3}
10^{-4}
10^{-5}
10^{-6}
10^{-7}
10^{-8}
10^{-9}
0
0.2
0.4
0.6
0.8
1.0
Overpotential (η volts)

FIG.2

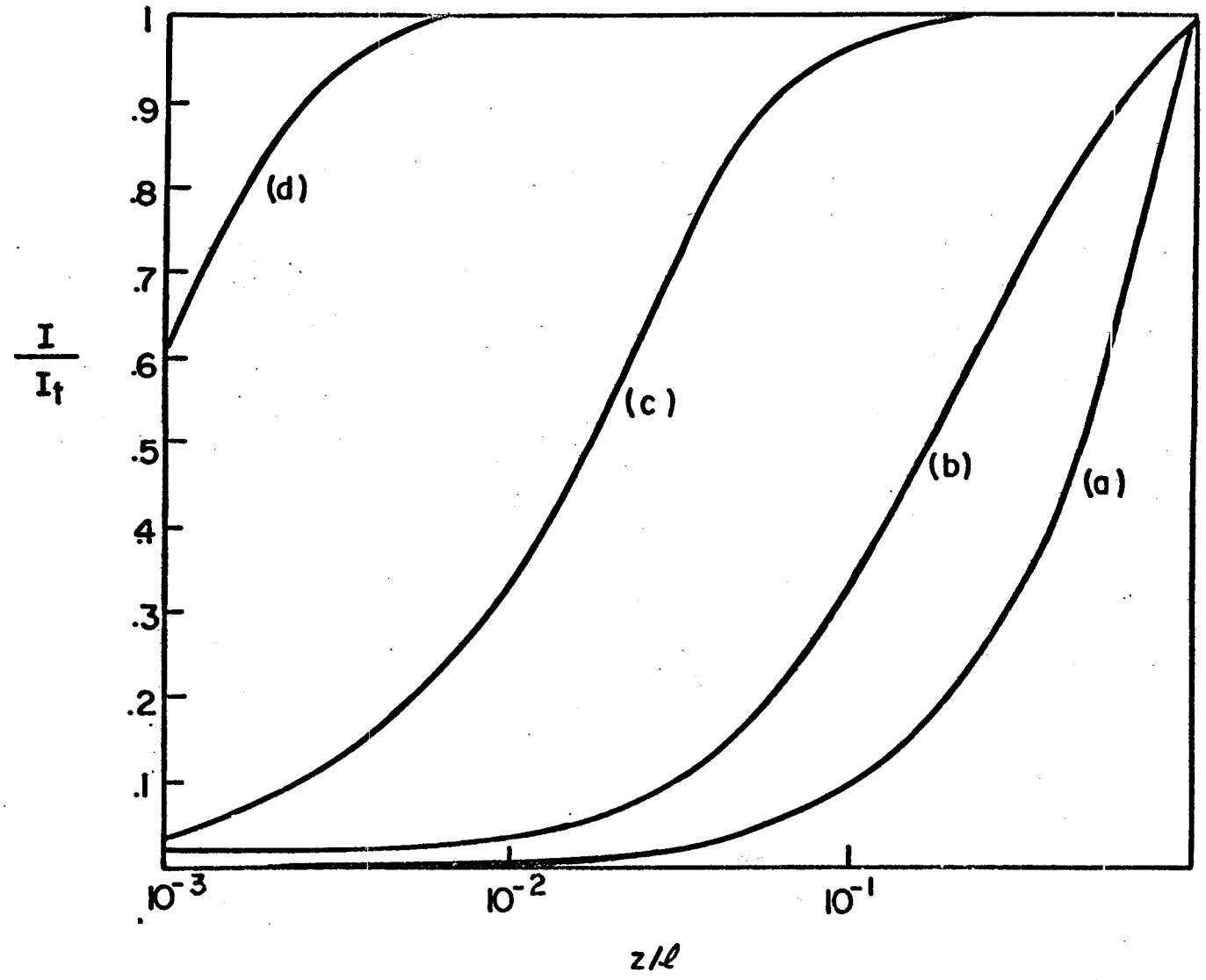

FIG.3

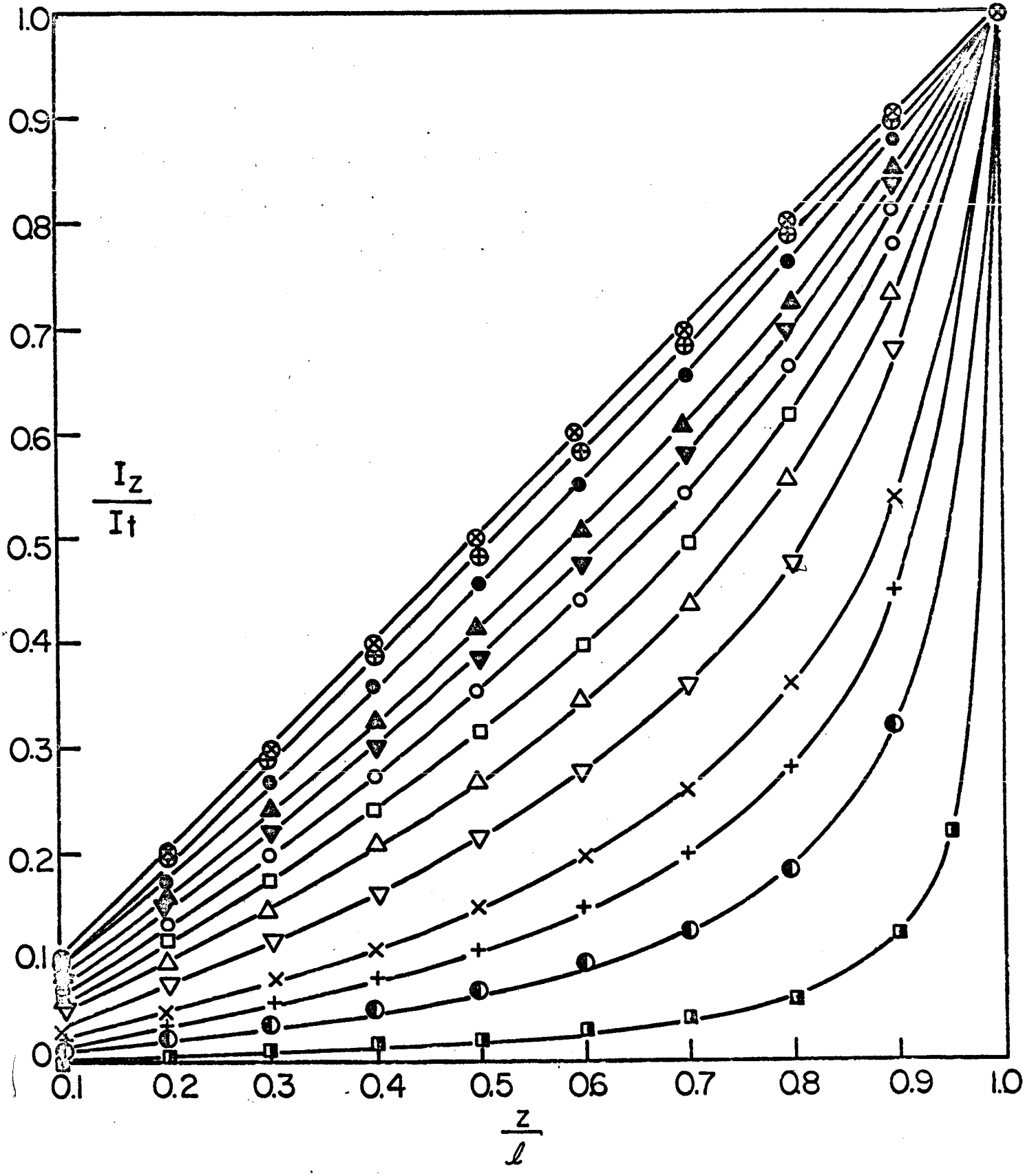
1.0
0.9
0.8
0.7
0.6
0.5
0.4
0.3
0.2
0.1
0
$\frac{I_z}{I_t}$
0.1
0.2
0.3
0.4
0.5
0.6
0.7
0.8
0.9
1.0
$\frac{z}{\ell}$

FIG. 4

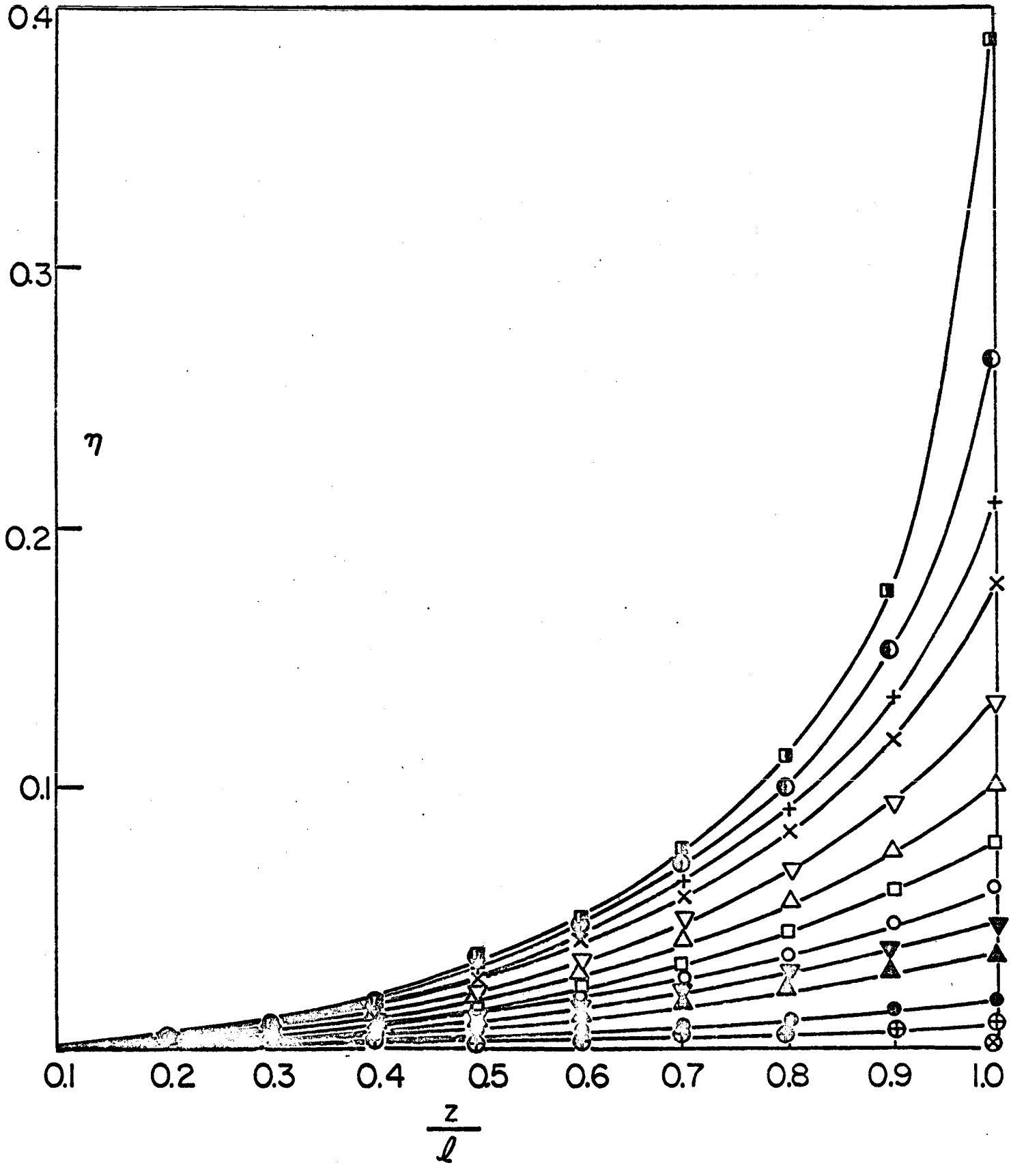

FIG. 5

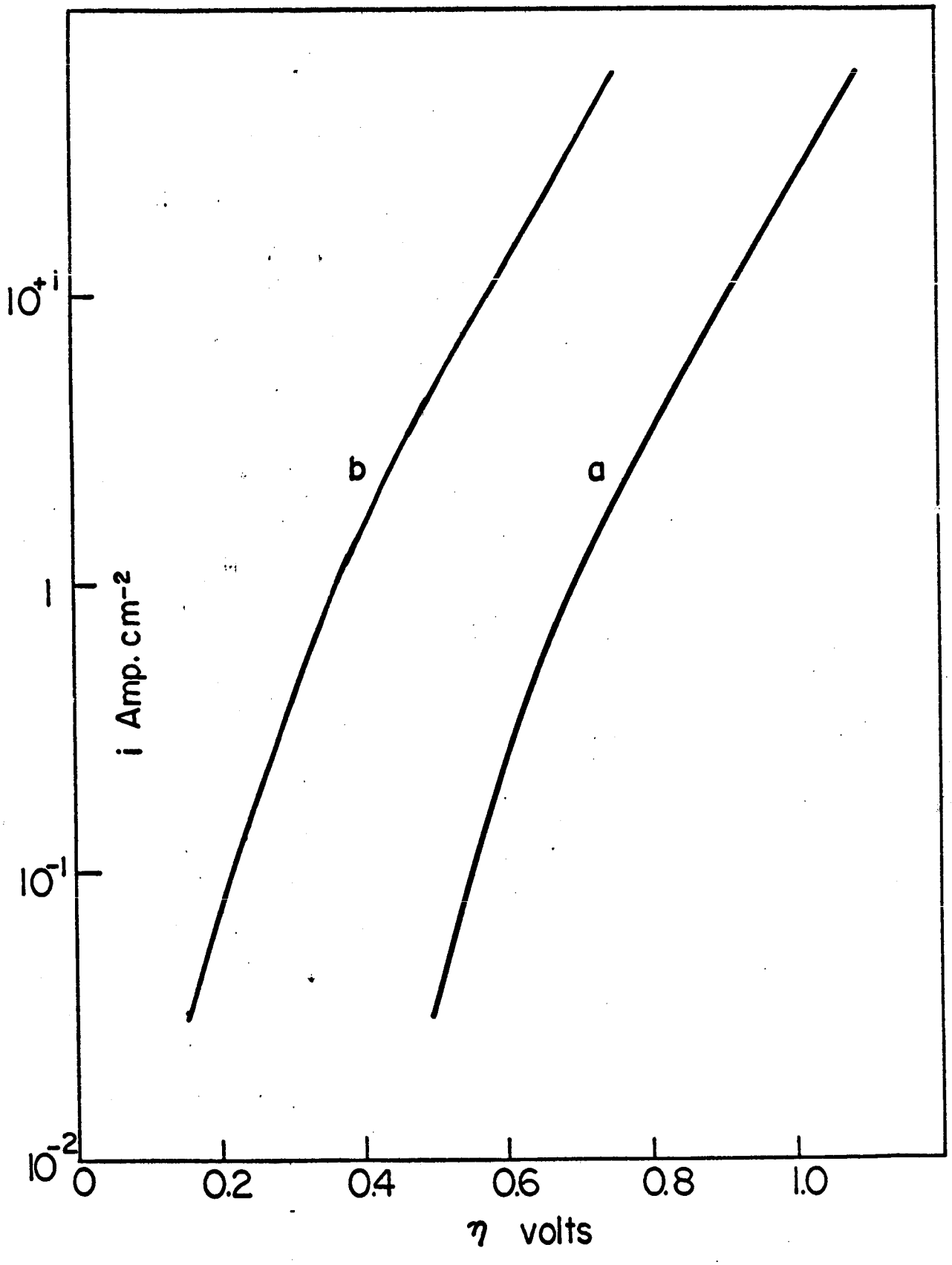

FIG. 6

VI. PUBLICATIONS UNDER GRANT NsG-325

1. Forces involved in the Specific Adsorption of Ions on metals from aqueous solution, J. O'M. Bockris and T. Anderson, Electrochimica Acta, 9, 347 (1964).

2. Electrochemical Kinetics of Parallel Reactions, E. Gileadi and S. Srinivasan, J. of Electroanal. Chem., 7 (1964) 452-457.

3. Electrocatalysis, J. O'M. Bockris and H. Wroblowa, J. Electroanal. Chem., 7 (1964) 428-451.

4. Basis of possible continuous self activation in an electrochemical energy converter, J. O'M. Bockris, B. J. Piersma, E. Gileadi and B. D. Cahan, J. Electroanal. Chem., 7 (1964) 487-490.

5. Ellipsometry in Electrochemical Studies, A. K. N. Reddy and J. O'M. Bockris, U. S. Dept. Comm. Natl. Bureau of Standards, Mics Publication 256, Sept. 15, 1964, 229-244.

6. Ellipsometric Study of oxygen-containing films on Platinum electrodes. A. K. N. Reddy, M. Genshaw and J. O'M. Bockris, J. Electroanal. Chem., 8 (1964) 406-407.

7. Ellipsometric Determination of the Film Thickness and Conductivity during the Passivation Process on Nickel, A. K. N. Reddy, M. G. B. Rao and J. O'M. Bockris, J. Chem. Phys., 42, 6, 2246-2248, 15 March 1965.

8. A Brief Outline of Electrocatalysis, J. O'M. Bockris and S. Srinivasan, 19th Annual Proceedings Power Sources Conference, May 1965.

9. Proton Transfer across Double Layers, J. O'M. Bockris, S. Srinivasan, and D. B. Matthews, Disc. Faraday Soc., 1965, No. 39.

The following are in course of publication

10. The Potential of Zero Charge on Pt and its pH Dependence, E. Gileadi, S. D. Argade and J. O'M. Bockris, J. Phys. Chem., in press.

11. The Potential Sweep Method: A Theoretical Analysis, S. Srinivasan and E. Gileadi, Electrochim. Acta, in press.

12. An ellipsometric study of oxide films on platinum in acid solutions, J. O'M. Bockris, A. K. N. Reddy and M. Genshaw.

13. Electrode Kinetic Aspects of Electrochemical Energy Conversion, J. O'M. Bockris and S. Srinivasan.

14. Electrocatalysis in Ethylene Oxidation, A. Kuhn, H. Wroblowa and J. O'M. Bockris.

VII. DISTRIBUTION LIST FOR FUEL CELL REPORTS

National Aeronautics & Space Administration
Washington, D. C. 20546
Attn: Ernst M. Cohn, Code RNW
George F. Esenwein, Code MAT
A. M. Andrus, Code ST
J. R. Miles, Code SL

National Aeronautics & Space Administration
Scientific and Technical Information Facility
P. O. Box 5700
Bethesda, Maryland, 20014 (3)

National Aeronautics & Space Administration
Goddard Space Flight Center
Greenbelt, Maryland
Attn: Thomas Hennigan

National Aeronautics & Space Administration
Langley Research Center
Langley Station
Hampton, Virginia
Attn: S. T. Peterson

National Aeronautics & Space Administration
Lewis Research Center
21000 Brookpark Road
Cleveland 35, Ohio
Attn: N. D. Sanders
Robert Miller
Robert L. Cummings

National Aeronautics & Space Administration
Marshall Space Flight Center
Huntsville, Alabama
Attn: Philip Youngblood

National Aeronautics & Space Administration
Ames Research Center
Pioneer Project
Moffett Field, California
Attn: James R. Swain

Cell Reports (con't)

National Aeronautics & Space Administration
Manned Spacecraft Center
Houston 1, Texas
Attn: Richard Ferguson (for EP-5)
Robert Cohen
Forrest E. Eastman, EE-4

National Aeronautics & Space Administration
Ames Research Center
Mountain View, California
Attn: Jon Rubenzer, Biosatellite Project

Jet Propulsion Laboratory
4800 Oak Grove Drive
Pasadena, California
Attn: Aiji Uchiyama

DEPARTMENT OF THE ARMY

U. S. Army Engineer R&D Labs.
Fort Belvoir, Virginia
Attn: Electrical Power Branch

U. S. Army Engineer R&D Labs.
Fort Monmouth, New Jersey
Attn: Arthur F. Daniel (Code SELRA/SL-PS)

U. S. Army R&D Liaison Group (9851 DV)
APO 757
New York, New York
Attn: Chief, Chemistry Branch

U. S. Army Research Office
Physical Sciences Division
3045 Columbia Pike
Arlington, Virginia

Harry Diamond Labs.
Room 300, Building 92
Connecticut Avenue & Van Ness Street, N.W.
Washington, D.C.
Attn: Nathan Kaplan

Cell Reports (con't.)

Army Material Command
Research Division
AMCRD-RSCM T-7
Washington 25, D.C.
Attn: John W. Crellin

Natick Labs.
Clothing & Organic Materials Div.
Natick, Massachusetts
Attn: Leo A. Spano/Robert N. Walsh

U. S. Army TRECOM
Physical Sciences Group
Fort Eustis, Virginia
Attn: (SMOFE)

U. S. Army Research Office
Box CM, Duke Station
Durham, North Carolina
Attn: Paul Greer/Dr. Wilhelm Jorgensen

U. S. Army Mobility Command
Research Division
Center Line, Michigan
Attn: O. Renius (AMSMO-RR)

Hq., U. S. Army Material Command
Development Division
Washington 25, D.C.
Attn: Marshall D. Aiken (AMCRD-DE-MO-P)

DEPARTMENT OF THE NAVY

Office of Naval Research
Department of the Navy
Washington 25, D. C.
Attn: Dr. Ralph Roberts/H.W. Fox

Cell Reports (con't.)

Mr. J. H. Harrison
Special Projects Division
U. S. Navy Marine Engineering Lab.
Annapolis, Maryland 21402

Bureau of Naval Weapons
Department of the Navy
Washington 25, D.C.
Attn: (Code RAAE)

U. S. Naval Research Laboratory
Washington, D.C., 20390
Attn: (Code 6160)

Bureau of Ships
Department of the Navy
Washington 25, D.C.
Attn: Bernard B. Rosenbaum/C. F. Viglotti

Naval Ordnance Laboratory
Department of the Navy
Corona, California
Attn: Mr. William C. Spindler (Code 441)

Naval Ordnance Laboratory
Department of the Navy
Silver Spring, Maryland
Attn: Philip B. Cole (Code WB)

DEPARTMENT OF THE AIR FORCE

Wright-Patterson AFB
Aeronautical Systems Division
Dayton, Ohio
Attn: George W. Sherman, APIP

AF Cambridge Research Lab
Attn: CRZE
L. G. Hanscom Field
Bedford, Massachusetts
Attn: Francis X. Doherty/Edward Rasking (Wing F)

Cell Reports (cont'd)

Rome Air Development Center, ESD
Griffiss AFB, New York
Attn: Frank J. Mollura (RASSM)

Space Systems Division
Attn: SSZAE-11
Air Force Unit Post Office
Los Angeles 45, California

Air Force Ballistic Missile Division
Attn: WEZYA-21
Air Force Unit Post Office
Los Angeles 45, California

ATOMIC ENERGY COMMISSION

Mr. Donald B. Hoatson
Army Reactors, DRD
U. S. Atomic Energy Commission
Washington 25, D. C.

OTHER GOVERNMENT AGENCIES

Office, DDR&E: USW & BSS
The Pentagon
Washington 25, D. C.
Attn: G. B. Wareham

Mr. Kenneth B. Higbie
Staff Metallurgist
Office, Director of Metallurgy Research
Bureau of Mines
Interiof Building
Washington, D. C., 20240

Institute for Defense Analyses
Research & Engineering Support Division
400 Army-Navy Drive
Arlington, Virginia 22202
Attn: Dr. George C. Szego/R. Hamilton

Cell Reports (cont'd)

Power Information Center
University of Pennsylvania
Moore School Building
200 South 33rd Street
Philadelphia 4, Pennsylvania

Chief, Input Section, CFSTI
Sills Building
5285 Port Royal Road
Springfield, Virginia, 22151

PRIVATE INDUSTRY

Alfred University
Alfred, New York
Attn: Professor T. J. Gray

Allis-Chalmers Mfg. Co.
1100 S. 70th Street
Milwaukee 1, Wisconsin
Attn: Dr. W. Mitchell, Jr.

Allison Division of General Motors
Indianapolis 6, Indiana
Attn: Dr. Robert E. Henderson

American Cyanamid Company
1937 W. Main Street
Stamford, Connecticut
Attn: Dr. R. G. Haldeman

American Machine & Foundry
689 Hope Street
Springdale, Connecticut
Attn: Dr. L. H. Shaffer
Research & Development Division

Cell Reports (cont'd.)

Astropower, Inc.
2968 Randolph Avenue
Costa Mesa, California
Attn: Dr. Carl Berger

Battelle Memorial Institute
Columbus 1, Ohio
Attn: Dr. C. L. Faust

Bell Telephone Laboratories, Inc.
Murray Hill, New Jersey
Attn: Mr. U. B. Thomas

Clevite Corporation
Mechanical Research Division
540 East 105 th Street
Cleveland, Ohio
Attn: A. D. Schwope

Electrochimica Corp.
1140 O'Brien Drive
Menlo Park, California
Attn: Dr. Morris Eisenberg

Electro-Optical Systems, Inc.
300 North Halstead Street
Pasadena, California
Attn: E. Findl

Engelhard Industries, Inc.
497 DeLancy Street
Newark 5, New Jersey
Attn: Dr. J. G. Cohn

Esso Research & Engineering Company
Products Research Division
P. O. Box 215
Linden, New Jersey
Attn: Dr. Carl Heath

Cell Reports (con'd.)

The Franklin Institute
Philadelphia, Pennsylvania
Attn: Mr. Robert Goodman

General Electric Company
Direct Energy Conversion Operations
Lynn, Massachusetts
Attn: Dr. E. Glazier

Garrett Corp.
1625 Eye St., N. W.
Washington 6, D. C.
Attn: George R. Shepherd

General Electric Company
Research Laboratory
Schenectady, New York
Attn: Dr. H. Liebhafsky

General Electric Company
Missile and Space Division (Room M133S)
P. O. Box 8555
Philadelphia 1, Pennsylvania
Attn: L. Chasen

General Motors Corp.
Box T
Santa Barbara, California
Attn: Dr. C. R. Russell

Globe-Union, Inc.
Milwaukee 1, Wisconsin
Attn: Dr. C. K. Morehouse

Dr. Joseph S. Smatko
General Motors
Defense Research Laboratories
P. O. Box T
Santa Barbara, California, 93102

Cell Reports (cont'd.)

John Hopkins University
Applied Physics Laboratory
8621 Georgia Avenue
Silver Springs, Maryland
Attn: W. A. Tynan

Leesona Moos Laboratories
Lake Success Park
Community Drive
Great Neck, New York
Attn: Dr. A. Moos

McDonnell Aircraft Corporation
Attn: Project Gemini Office
P. O. Box 516
St. Louis 66, Missouri

Monsanto Research Corporation
Everette 49, Massachusetts
Attn: Dr. J. O. Smith

North American Aviation Co.
S & ID Division
Downey, California
Attn: Dr. James Nash

Pratt and Whitney Aircraft Division
United Aircraft Corporation
East Hartford 8, Connecticut
Attn: Librarian

Radio Corporation of America
Astro Division
Heightstown, New Jersey
Dr. Seymour Winkler

Radio Corporation of America
Somerville, New Jersey
Attn: Dr. G. Lozier

Cell Reports (cont'd.)

Speer Carbon Company
Research And Development Laboratories
Packard Road at 47th Street
Niagara Falls, New York
Attn: Dr. L. M. Liggett

Stanford Research Institute
820 Mission Street
So. Pasadena, California
Attn: Dr. Fritz Kalhammer

Thiokol Chemical Corporation
Reaction Motors Division
Denville, New Jersey
Attn: Dr. D. J. Mann

Thompson Ramo Wooldridge
2355 Euclid Avenue
Cleveland 17, Ohio
Attn: Mr. Vittor Kovacik

Unified Science Associates, Inc.
826 S. Arroyo Parkway
Pasadena, California
Attn: Dr. Sam Naiditch

Union Carbide Corporation
12900 Snow Road
Parma, Ohio
Attn: Dr. George E. Evans

University of California
Space Science Laboratory
Berkeley 4, California
Attn: Prof. Charles W. Tobias

University of Pennsylvania
Philadelphia 4, Pennsylvania
Attn: Dr. Manfred Altman

Cell Reports (cont'd.)

Western Reserve University
Cleveland, Ohio
Attn: Prof. Ernest Yeager

Yardney Electric Corp.
New York, New York
Attn: Dr. Paul Howard

Lockheed Missiles & Space Co.
3251 Hanover St.
Palo Alto, California
Attn: Dr. George B. Adams

Mr. B. S. Baker
Institute of Gas Technology
State & 34th Streets
Chicago 16, Illinois

Mr. Peter D. Richman
President
Chem Cell Inc.
3 Central Ave.
East Newark, New Jersey 07029